iScience

CellPress
OPEN ACCESS

Article

Estimation of activity coefficients for aqueous organic redox flow batteries: Theoretical basis and equations

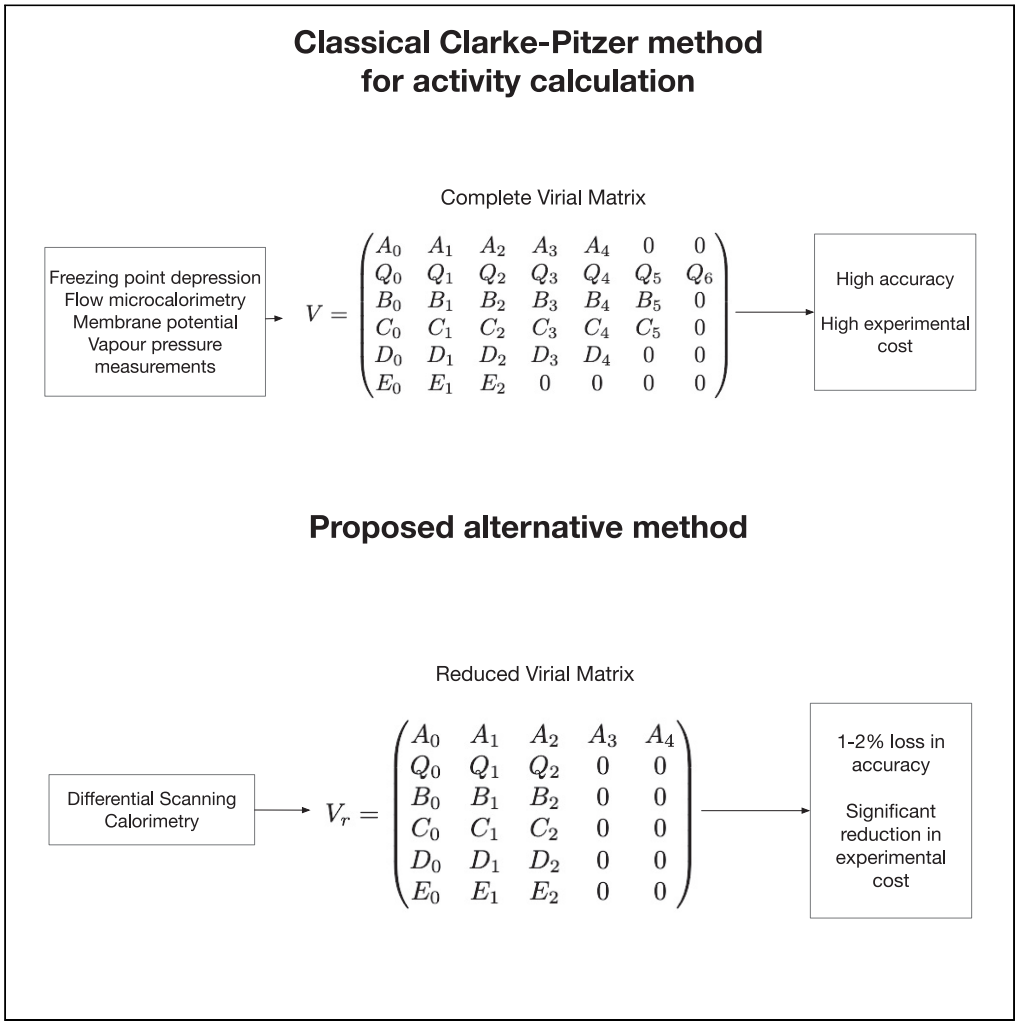

Gaël Mourouga, Déborah Chery, Emmanuel Baudrin, Hyacinthe Randriamahazaka, Thomas J. Schmidt, Juergen O. Schumacher

gaelmourouga@protonmail.com

Highlights

This article reviews the use of concentrated solution theory in flow batteries

The virial matrix method for estimating activity coefficients is proposed

Its high accuracy and experimental costs are underlined

A novel method, the reduced virial matrix, is proposed

Mourouga et al., iScience 25, 104901
September 16, 2022
https://doi.org/10.1016/j.isci.2022.104901

iScience

CellPress
OPEN ACCESS

Article

Estimation of activity coefficients for aqueous organic redox flow batteries: Theoretical basis and equations

Gaël Mourouga,[1,7,*] Déborah Chery,[2] Emmanuel Baudrin,[3] Hyacinthe Randriamahazaka,[4] Thomas J. Schmidt,[5,6] and Juergen O. Schumacher[1]

SUMMARY

The field of aqueous organic redox flow batteries (AORFBs) has been developing fast in recent years, and many chemistries are starting to emerge as serious contenders for grid-scale storage. The industrial development of these systems would greatly benefit from accurate physics-based models, allowing to optimize battery operation and design. Many authors in the field of flow battery modeling have brought evidence that the dilute solution hypothesis (the assumption that aqueous electrolytes behave ideally) does not hold for these systems and that calculating cell voltage or chemical potentials through concentrations rather than activities, while serviceable, may become insufficient when greater accuracy is required. This article aims to provide the theoretical basis for calculating activity coefficients of aqueous organic electrolytes used in AORFBs to provide tools to predict the concentrated behavior of aqueous electrolytes, thereby improving the accuracy of physics-based models for flow batteries.

INTRODUCTION

Among energy storage technologies, batteries have recently seen a surge in popularity, owing to their flexibility of installation and lower capital costs required compared with larger centralized storage technologies, allowing the transition from a centralized grid model to that of a network of smart, decentralized microgrids (Gür, 2018). In this context, aqueous organic redox flow batteries (AORFBs) present a number of significant advantages, including: absence of metal-based active materials, leading to a greener and more resilient supply chain of battery materials when compared to metal-based technologies; decorrelation between energy and power sizing, leading to a greater flexibility in design to meet local grid requirements; and finally non-flammability because of the large volumes of water-based electrolytes, leading to a greater reliability compared to technologies presenting the risk of thermal runaway (lithium-ion) or high flammability (hydrogen).

Flow batteries and concentrated solution theory

Since the first modeling studies conducted by NASA (Fedkiw and Watts, 1984), computational models have become increasingly important for optimizing operating and design parameters of the batteries. Although it is common practice to assume the aqueous electrolyte solutions flowing in the battery to be ideal, i.e., where the ions are assumed not to interact with each other (the dilute solution hypothesis), a growing number of authors are opposing this hypothesis, advocating for using concentrated solution theory instead, which accounts for non-idealities of mixing. In order to assess the current state of the literature consensus on the topic, we conducted a meta-analysis on a literature sample (N = 66) focusing on the development of computational models for redox-flow batteries. Based on the featured equations and their hypotheses and justifications, papers were classified in four categories.

In category A, equations featured uncorrected concentrations (e.g., in voltage predictions), but the dilute solution hypothesis was not mentioned explicitly. As an illustration, You et al. (2009) manipulated concentrations to calculate the open-circuit potential (OCP) of an electrode as

$$U_{OCP} = U^0 + \frac{RT}{F}\ln\left(\frac{c_{red}}{c_{ox}}\right), \qquad \text{(Equation 1)}$$

[1]Institute of Computational Physics, ZHAW, Wildbachstr. 21, 8400 Winterthur, Switzerland

[2]Université d'Angers, Faculté des Sciences, 2 boulevard Lavoisier, 49045 Angers, France

[3]Laboratoire de Réactivité et Chimie des Solides (LRCS), UMR CNRS 7314, Université de Picardie Jules Verne, 33 rue Saint-Leu, 80039 Amiens Cedex, France

[4]Université de Paris Cité, CNRS, ITODYS, 75013 Paris, France

[5]Paul Scherrer Institut, Electrochemical Laboratory, Forschungsstrasse 111, CH-5232 Villigen PSI, Switzerland

[6]ETH Zurich, Laboratory for Physical Chemistry, CH-8092 Zurich, Switzerland

[7]Lead contact

*Correspondence: gaelmourouga@protonmail.com

https://doi.org/10.1016/j.isci.2022.104901

where U^0 is the reference thermodynamic potential (V vs. SHE), R the ideal gas constant, T the absolute temperature, F Faraday's constant and c_{red} and c_{ox} (mol/L) the concentrations of reduced and oxidized species, respectively, of the redox pair in the considered electrode. You et al. (2009) noted that "*a total value of 140 mV was added to the simulated results in order to match the experimental data*" but the fact that this voltage discrepancy may arise from the hypothesis of ideal solutions was not mentioned.

In category B, the dilute solution hypothesis was mentioned explicitly: For example, Shah et al. (2011) mention that "*concentrated-solution theory is straightforward but […] several parameters are not known for the present system*" so that as in You et al., "*A total value of 131 mV was [added] from fitting the experimental data to simulation results*".

In category C, authors either attempted to justify the dilute solution hypothesis, or at least question its validity. Knehr and Kumbur (2011) belong to the former category, with very debatable justifications e.g., "*in a VRFB, the liquid electrolytes are typically well-circulated, yielding negligible interactions among the ions*". They did rightly, however, introduce an additional term in the open-circuit potential to account for possible imbalances in the concentration of supporting ions

$$U_{OCP} = U^0 + \frac{RT}{F} \ln \prod_{i=1}^{N} c_i^{\nu_i}, \qquad \text{(Equation 2)}$$

where c_i corresponds to the concentration of species and ν_i to their stoichiometric coefficient in the half-cell reaction, including exchanged ions (protons in the case of Knehr and Kumbur (2011)). Stephenson et al. (2012) instead acknowledged that standard potentials in the Nernst equation may be shifted from non-ideal effects "*Like Shah* et al.*[…] we also observed a shift in equilibrium potential. It may be attributed to the non-ideal solution, in which the activity coefficient is not equal or close to one.*" leading to the first mention of the possibility that activity coefficients may deviate from their ideal value in flow batteries since Heintz and Illenberger (1998). No attempt was made, however, at quantifying these activity coefficients and the discrepancies arising from the behavior of non-ideal solutions.

In category D, authors attempted to manipulate equations in accordance with concentrated solution theory and sometimes advocated against the dilute solution hypothesis. Hayer and Kohns (2020) for example state that "*fitting kinetic parameters to measurement data of voltage losses can lead to ambiguous results if only the idealized OCV, obtained by neglecting the activity coefficients, is used in that evaluation*" and therefore re-introduce the more fundamental form of the Nernst equation for the calculation of the open-circuit voltage

$$U_{OCP} = U^0 - \frac{RT}{F} \ln \prod_{i=1}^{N} a_i^{\nu_i}, \qquad \text{(Equation 3)}$$

where a_i corresponds the chemical activity of species in the electrodes, a quantity central to concentrated solution theory, which will be the focus of the present publication.

It seems apparent from the visualization of the dilute versus concentrated debate on Figure 1 that although the dilute solution hypothesis was very prevalent between 2000 and 2010 (category A + B), a few papers started either questioning the assumptions behind it, or at least acknowledging that the dilute solution hypothesis should be justified (category C), between 2010 and 2018. Although a few papers re-introduced the notion of chemical activity (which was present in the paper from Heintz and Illenberger (1998) but considered negligible in the following decade), a vast majority of the literature preferred the use of concentration. Between 2018 and today, however, it seems that the literature reviewed in this analysis has polarized into two main schools of thoughts: On the one hand, papers using concentrations in their parametrization, not mentioning the dilute solution hypothesis and its implications, and on the other hand authors advocating for the manipulation of equations in line with concentrated solution theory.

Activity coefficients impact the OCV of the cell and typically introduce a few tens of mV of discrepancy with the same equations parametrized with concentrations (Hayer and Kohns, 2020; del Olmo et al., 2021; Mourouga et al., 2022). Although this value may sound negligible for performance models over a single cycle,

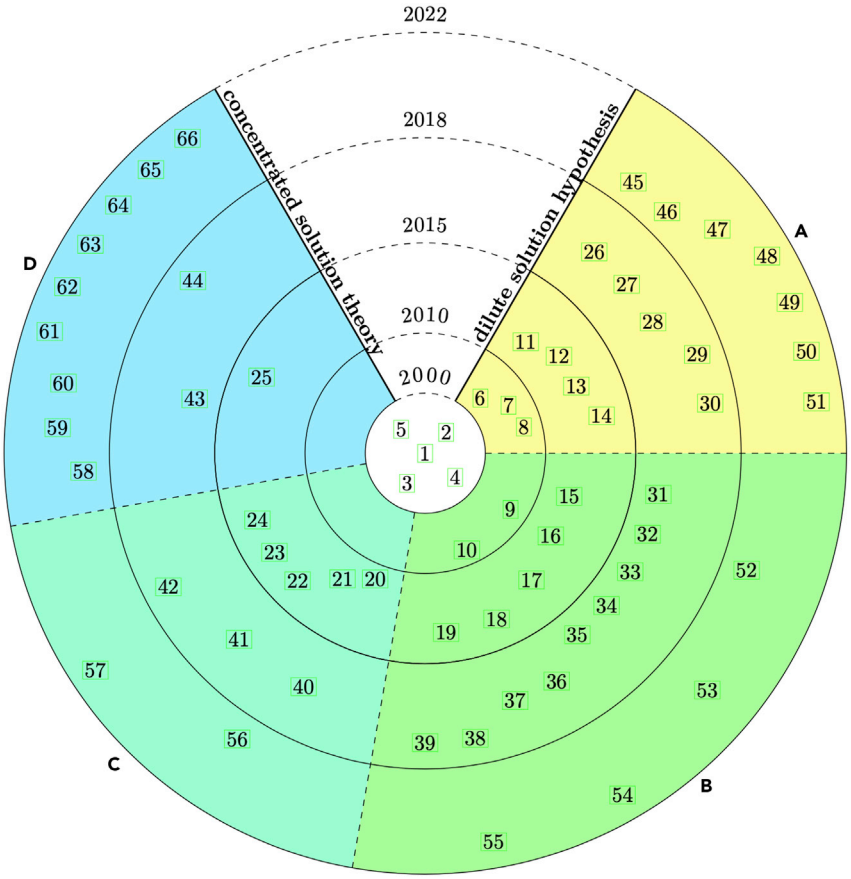

Figure 1. Visual representation of the dilute vs. concentrated debate in flow battery modeling literature

Papers are ordered in 4 categories. (A) Papers using the dilute solution hypothesis without mentioning it; 2000–2010: [6] Sukkar and Skyllas-Kazacos (2003), [7] Li and Hikihara (2008), [8] You et al. (2009); 2010–2015: [11] Tang et al. (2011), [12] Qiu et al. (2012), [13] Tang et al. (2012), [14] Badrinarayanan et al. (2014); 2015-2018: [26] Zhou et al. (2016), [27] Nikonenko et al. (2016), [28] Yan et al. (2016), [29] Milshtein et al. (2017), [30] Bhattacharjee and Saha (2017); 2018-2022: [45] Lei et al. (2018), [46] Murali et al. (2018), [47] Chen et al. (2019) [48] Xu et al. (2020) [49] Chen et al. (2021a), [50] Chen et al. (2021b) [51] Howard Amanda and Tartakovsky (2021).

(B) Papers mentioning the dilute solution hypothesis but not justifying it; 2000–2010: [9] Shah et al. (2008), [10] Al-Fetlawi et al. (2009); 2010–2015: [15] Shah et al. (2011), [16] Vynnycky (2011), [17] Knehr et al. (2012), [18] Yin et al. (2014) [19] Chen et al. (2014); 2015-2018: [31] Xu and Zhao (2015), [32] Yang et al. (2015), [33] Boettcher et al. (2015), [34] Zhou et al. (2015), [35] Lei (2015), [36] Gandomi et al. (2016), [37] Chu et al. (2016), [38] Chen et al. (2017), [39] Elgammal et al. (2017); 2018-2022: [52] Ronen et al. (2018), [53] Oh et al. (2019), [54] Delgado et al. (2020), [55] Cacciuttolo et al. (2021).

(C) Papers justifying or discussing the dilute solution hypothesis; 2010–2015: [20] Knehr and Kumbur (2011), [21] Stephenson et al. (2012), [22] Wandschneider et al. (2014), [23] Hudak (2014), [24] Wei et al. (2014); 2015-2018: [40] Darling et al. (2016), [41] Darling et al. (2016), [42] Moshtarikhah et al. (2017); 2018-2022 [56] Murthy et al. (2018) [57] Al-Yasiri (2020).

(D) Papers using equations coherent with concentrated solutions theory; 2010-2015: [25] Ashraf Gandomi et al. (2014); 2015–2018: [43] Pavelka et al. (2015), [44] Xu et al. (2017); 2018-2022: [58] Intan et al. (2018), [59] Sijabat et al. (2019), [60] Hao et al. (2019), [61] Kleinsteinberg et al. (2020), [62] Hayer and Kohns (2020), [63] del Olmo et al. (2020), [64] Crothers et al. (2020) [65] Vardner et al. (2020) [66] Mourouga et al. (2022). Distance from the center and clockwise angle are proportional the publication date. The 5 earliest publications (Reid and Gahn (1977), Fedkiw and Watts (1984), Zawodzinski et al. (1993), Mohammadi et al. (1997), Heintz and Illenberger (1998)) are shown for reference but were not categorised.

modeling a flow battery over several thousands of charge-discharge cycles requires accurate transport models. Transport models, in turn, are highly impacted by the chemical potentials of species mixing in the battery, which are directly impacted by thermodynamic activity according to the formula

$$\mu_i - \mu_i^0 = RT \ln a_i, \qquad \text{(Equation 4)}$$

where μ_i is the chemical potential, μ_i^0 is a reference chemical potential in standard conditions and a_i is the thermodynamic activity, capturing interactions in highly concentrated solutions.

In addition to chemical potentials, transport models are also highly impacted by cycling times which, in turn, correspond to the time at which the cell voltage reaches its cut-off values. Therefore, uncertainties of a few tens of mV on the cell voltage will result in a few minutes of uncertainty on the first cycling time, which will quickly propagate to several hours over thousands of cycles. Accurate OCV calculations, using activity estimation as in Equation (3) rather than concentrations as in Equation (2), thus significantly improve the accuracy of flow battery models over long time scales.

Furthermore, thermodynamic activity also impacts other characteristics of the electrolytes, such as their conductivity and heat capacities. Accurate physics-based shunt currents and thermal models therefore also greatly benefit from accurate activity coefficient values over a wide range of composition and temperature.

To the best of our knowledge, no publication has so far addressed the problem of measuring activity coefficients of flow battery electrolytes, especially for aqueous organic redox-flow batteries. The estimation of activity coefficients for flow batteries will therefore be the focus of this series of publication, in which the present one will introduce the theoretical foundation for the calculation of activity coefficients from experimental data on the properties of solutions.

A short history of activity

The term *chemical activity* was first coined by Lewis (1907) at a time where two different approaches were competing for predicting observable properties of aqueous electrolytes such as vapor pressure, osmotic pressure, and freezing point. The first one was led by Van't Hoff, Nernst, and Arrhenius and aimed to apply laws demonstrated from the kinetic theory of ideal gases to chemical systems, whereas the second one, led by Gibbs (1879), Duhem, Planck and Lewis aimed to apply the fundamental laws of physics and thermodynamics to chemical systems.

The main difference between the two approaches lies in how they express the chemical potential of solutes dissolved in a solvent: The kinetic theory of ideal solutions approach relies on the assumption that charged particles in an aqueous solution behave similarly to ideal gases, which allows to express the chemical potential as a function of the logarithm of the molality b (in moles of solute per kilogram of solvent)

$$\mu_i - \mu_i^0 = RT \ln\left(\frac{b_i}{b_i^0}\right), \qquad \text{(Equation 5)}$$

where μ_i^0 is a chemical potential taken in standard conditions of pressure and temperature, and b_i^0 is a standard molality, chosen as 1 mol kg^{-1} for convenience.

The approach championed by Lewis, on the other hand, defines the notions of *chemical activity* a_i, which is equal to the molality multiplied by an *activity coefficient* γ_i accounting for interactions between the mixing species

$$\mu_i - \mu_i^0 = RT \ln\left(\gamma_i \frac{b_i}{b_i^0}\right). \qquad \text{(Equation 6)}$$

It should be noted that the standard state and standard molality have the same physical meaning in both frameworks: they represent the hypothetical case of an ideal (non-interacting) mixture at a molality of one mole of solute per kilogram of solvent. Any calculated chemical potential is therefore a deviation from this ideal state, which follows from the fact that only differences in Gibbs free energy ΔG between two thermodynamic states, as opposed to absolute Gibbs free energies G, are measurable.

Debye and Hückel (1923) provided the first theoretical calculation of activity coefficients, coherent with experimental measurements in dilute solutions. Their main idea was that charged ions obeyed the law of electrostatic interactions, and that through the application of the Boltzmann principle and the Poisson equation, one could derive the changes in potential energy of ionic solutions and thus, predict measurable quantities such as freezing point depression: *For all electrolytes, in the limit for low concentrations, the percentage deviation of the freezing point depression from the classical value is proportional to the square*

root of the concentration. This theorem (and the two that follow, see Debye et al. (1923) for the English translation) constitute the Debye–Hückel limiting law and state that in the limit of low concentrations, activity coefficients can be interpreted as the influence of the electrostatic interaction on electrolyte solutions (Hückel and Braus, 2020).

Scatchard (1936) corrected some assumptions from the Debye–Hückel theory and replaced the use of concentrations c (moles of solute per volume of solution) with molalities b (moles of solute per mass of solvent), then Guggenheim (1935) and Guggenheim and Prue (1954) demonstrated the relationship between chemical activity and other properties of aqueous electrolytes, including enthalpies of mixing and heat capacity. Guggenheim and Turgeon (1955) further cemented the idea that higher order interactions were in play in more concentrated solutions.

The most general theory was demonstrated by Pitzer (1973), who showed that the virial theorem could be applied to aqueous electrolyte solution, leading to an expansion of the osmotic pressure and the excess Gibbs free energy (and thus, interactions) in powers of the molality b. Within this framework, activity coefficients can be viewed as an expression of different interactions in solution: $\gamma < 1$ represents overall repulsive (long-range) interactions, and $\gamma > 1$ represents overall attractive (higher-order, short-range) interactions. The higher-order interactions become dominant when the average distance between molecules is reduced, which therefore come to dominate in concentrated solutions.

The very extensive work of Pitzer and his successors (Pitzer and Mayorga (1973); Bradley and Pitzer (1979); Clarke and Glew (1966); Clarke and Glew (1980); Clarke and Glew (1985); Craft and Van Hook 1975a; Craft and Van Hook 1975b; Tanner and Lamb (1978); Fortier et al. (1973)) solidified his thermodynamic derivations and validated them with vapor pressure, liquid junction potential and calorimetry measurements on many different aqueous solutions and mixtures. Although this approach allows to derive relationships between properties of a mixture that could appear disconnected (osmotic pressure and excess heat capacity for example), it should be emphasized that it remained a semi-empirical approach, where many phenomenological coefficients had to be fitted to experimental results in order to achieve a satisfying predicting power.

Other mathematical frameworks relying on the calculation of the excess Gibbs free energy of a mixture, but with an emphasis on computation rather than experimentation, emerged after the theory of Pitzer, such as the universal quasi-chemical equation (UNIQUAC) developed by Abrams and Prausnitz (1975) and extended by other authors to UNIFAC (Fredenslund et al., 1975; Maurer and Prausnitz, 1978) or GEQUAC (Egner et al., 1997).

According to Abrams and Prausnitz themselves *"the UNIQUAC equation gives good representation of both vapor-liquid and liquid-liquid equilibria for binary and multicomponent mixtures containing a variety of nonelectrolyte components such as hydrocarbons, ketones, esters, amines, alcohols, nitriles, etc …"*.

Other computational methods, such as COSMO (Klamt and Schüürmann, 1993) which later branched into COSMO-RS (Klamt, 1995) and COSMOSPACE (Klamt et al., 2002), were developed to bridge macroscopic statistical thermodynamics and quantum chemistry. Quantum chemistry is a fast-developing and exciting field, and future models may hold very real interests for the development of flow batteries, such as screening of new molecules or non-aqueous solvents.

In the present work, however, it was chosen to favor the semi-empirical approach of Pitzer-Clarke to estimate activity coefficients, as the focus of our work was to compute the properties of available flow battery electrolytes from a set of experiments. In the more general case where novel organic electrolytes would be investigated *in silico*, this approach might prove insufficient to screen the most promising electrolytes among a set of molecules. It is, however, undeniably the most accurate, provided experiments can be readily performed on the aqueous solutions and mixtures (Klamt et al., 2002).

CALCULATION OF ACTIVITY COEFFICIENTS

We will use the approach developed by Pitzer (1973) and Clarke and Glew (1966) to demonstrate a combined experimental and computational method for the estimation of activity coefficients from infinitely dilute solution to saturation, and a range of temperature ranging from 0 to 60°C, at atmospheric pressure, from selected experimental data of measurable properties of aqueous solutions.

Ideal solution model

Let us consider an aqueous solution system comprised N_s moles of an X_pY_q solute dissolved in N_w moles of water. The solute molality b, in moles of solute per kilogram of solvent, is defined as

$$b = 1000\frac{N_s}{N_w M_w}, \quad \text{(Equation 7)}$$

where M_w is the molar mass of water expressed in g/mol. Because it is assumed that the X_pY_q solute dissolves into pX^+ cations and qY^- anions the individual ionic molalities are defined as

$$b = \frac{b_+}{p} = \frac{b_-}{q}, \quad \text{(Equation 8)}$$

and the ionic strength I of the system is defined as

$$I = \frac{1}{2}\sum_i z_i b_i^2, \quad \text{(Equation 9)}$$

where z_i is the valence of ionic species dissolved in solution and b_i their molality. In the case of an ideal solution, it is assumed that the solute is fully dissociated and that the ions do not interact with each other (through electrostatic or Van Der Waals interactions, for example).

Within this framework, the kinetic theory of ideal gases developed by Maxwell and Boltzmann in the 1870s should be applicable to aqueous solutions, and their colligative properties (the osmotic pressure Π in Pa, the ionic conductivity σ in S/m, etc …) should be correlated with the molality b.

Experimental deviations from the ideal solution model

The osmotic pressure of aqueous solutions was shown by Van't Hoff in 1887 to follow the relationship

$$\Pi = iRTb, \quad \text{(Equation 10)}$$

Where R is the ideal gas constant, T the temperature, b the molality of solute and i the Van't Hoff number.

Van't Hoff showed that within an ideal solution framework, i should be equal to the number of ions the solute dissociates into $(p + q)$, but his experimental measurements pointed towards non-constant values for i, below that of the expected value at low concentrations and greater at high concentrations. Similar deviations from ideality would be observed by Arrhenius in 1884 (Hingerl, 2012) on the electrical conductivity of solutions, by Jones and Getman (1903) on their freezing point depression and by Marshall (1906) on their vapor pressure at saturation. Lewis and Randall (1921) challenged the values of the equilibrium constants measured by Guldberg and Waage in their law of mass action reported in 1899: "*to those who have not examined this question closely, it may be surprising to learn how far K_e [the equilibrium constant] is from being a constant*". He would be the first to formally introduce the notion of the activity coefficient γ_s, a mathematical function lower than 1 at low concentrations and greater than 1 at higher concentrations, to correct the "apparent molality" of solute and capture the non-linearities observed experimentally on the colligative properties of solution.

Using modern notations, the introduction of the osmotic coefficient φ (proportional to the activity of water and related to γ_s through the Gibbs-Duhem equation) in the law demonstrated by Van't Hoff, allows to calculate the observed deviation from ideality of the osmotic pressure with a simple expression

$$\Pi = (p + q)\varphi RTb, \quad \text{(Equation 11)}$$

In the general case, the Van't Hoff number i is therefore equal to $(p + q)\varphi$, and in the particular case of ideal solutions where $\varphi = 1$, we obtain the real number of ions the solute dissociates into $(p + q)$, as demonstrated by Van't Hoff in 1887.

Activity, Gibbs free energy of solutions and chemical potential

In 1873, Gibbs introduced the notion of Gibbs free energy G of a solution to quantify the amount of useful work which could be extracted from it, and the notion of chemical potential μ (molar free energy) to quantify how the available energy would evolve as a function of the number of moles of each component. For the aqueous solution previously defined (as demonstrated in A)

$$G = (p + q)N_s\mu_s + N_w\mu_w, \quad \text{(Equation 12)}$$

where $(p+q)N_s$ is the total number of mole of ions in solution, μ_s the chemical potential of the solute, N_w the number of moles of water and μ_w its chemical potential.

Lewis would build on the work of Gibbs in 1907 by decomposing the Gibbs free energy of solution as the sum of two terms: the ideal Gibbs free energy G^{id}, capturing the ideal solution behavior as predicted by the kinetic theory of gases, and the apparent molal excess Gibbs free energy G^{φ}, capturing the observed deviations from ideal solution behavior:

$$G = G^{id} + N_s G^{\varphi}, \quad \text{(Equation 13)}$$

where G^{φ} can be demonstrated to be proportional to the activity coefficient γ and osmotic coefficient φ according to the relationship (Clarke and Glew, 1985)

$$G^{\varphi} = (p+q)RT(1-\varphi+\ln\gamma_s). \quad \text{(Equation 14)}$$

More details on the derivation of Equation (12) and Equation (14) can be found in Appendix.

Continuum model of non-ideal solutions

It was shown by Pitzer (1973) that the behavior of ions dissolved in a solvent could be approached by considering interacting charged hard spheres (the ions) in a continuous medium (the solvent). In this framework, the average over time of the total kinetic energy of the ions, bound by long-range electrostatic interactions and short-range van der Waals interactions, was related to that of the total potential energy of the solution (its Gibbs free energy) through the virial theorem. This resulted in a development of the osmotic pressure and the Gibbs free energy of solution in powers of the molality b, which would allow to calculate the coefficients φ and γ_s accurately as a function of composition.

Virial expansion of the osmotic pressure

The virial expansion applied to the osmotic coefficient would yield the following dependence (Pitzer and Mayorga, 1973):

$$\varphi = 1 - |z_+ z_-| A \frac{I^{1/2}}{1+1.2I^{1/2}} + \left(\frac{2pq}{p+q}\right) e^{-2I^{1/2}} Qb + \left(\frac{2pq}{p+q}\right) Bb + \left(\frac{2(pq)^{3/2}}{p+q}\right) Cb^2 + \ldots \quad \text{(Equation 15)}$$

Where coefficient A is derived from the Debye–Hückel theory and only depends on the solvent, and the following terms (coefficients Q, B, C, D, E, …) are virial coefficients corresponding to solute interactions (e.g., electrostatic or van der Waals), developed in powers of the molality b. The Pitzer theory does not provide a framework for the calculation *in silico* of the virial coefficients, which need to be fitted to experimental data.

From the Gibbs–Duhem equation explicited in Appendix, it can be demonstrated that the dependency of the activity coefficient of solute γ_s with the molality b follows the relationship

$$\ln\gamma_s = -|z_+ z_-| A \left(\frac{I^{1/2}}{1+1.2I^{1/2}} + \frac{2}{1.2}\ln\left(1+1.2I^{1/2}\right)\right) + \frac{pq}{I(p+q)}\left(1 - e^{-2I^{1/2}}\left(1+2I^{1/2}-2I\right)\right) Qb + 2\left(\frac{2pq}{p+q}\right) Bb + \frac{3}{2}\left(\frac{2(pq)^{3/2}}{p+q}\right) Cb^2 + \ldots \quad \text{(Equation 16)}$$

by inserting Equation (15) and Equation (16) in Equation (14), we get the following expression for the apparent molal excess Gibbs free energy

$$G^{\varphi} = |z_+ z_-| A \frac{4I}{1.2b}\ln\left(1+1.2I^{1/2}\right) + \frac{pq}{I}\left[1 - \left(1+2I^{1/2}e^{-I^{1/2}}\right)\right] Qb + pqBb + \frac{1}{2}(pq)^{3/2} Cb^2 + \ldots \quad \text{(Equation 17)}$$

In short, once the Pitzer coefficients B, Q, C, D, … are known, they allow to calculate the variations of the excess Gibbs free energy, the activity coefficient, and the osmotic coefficient as a function of the molality b. This, in turn, allow to accurately capture experimental non-linearities observed in the osmotic pressure, the ionic conductivity, the freezing point depression or the vapor pressure of aqueous electrolyte solutions as a function of composition.

However, the values of the coefficients A, B, Q, C, D, …in Equations 15–17 as reported in Pitzer and Mayorga (1973), are given at 25°C. Although colligative properties of aqueous solutions, such as the ionic conductivity or the osmotic pressure, are not constant with temperature, the Pitzer coefficients should also exhibit variations with the temperature. This dependence was further investigated by a few authors (Cepeda, 1977; Phutela and Pitzer, 1986) and can be linked to the excess enthalpy of solution via a Taylor expansion in the neighborhood of a reference temperature.

Taylor expansion of the excess enthalpy

When mixing two non-ideal solutions of different compositions, an amount of heat, proportional to the enthalpy of mixing, is generated. Similarly, the heat capacity of the solution varies as a function of the composition and the temperature, in a way which is related to the enthalpy of mixing. Both phenomena are fundamentally related to the interactions between ions in solution and therefore, to the excess Gibbs free energy of the mixture.

Clarke and Glew (1966) demonstrated that the enthalpy of mixing ΔH^{φ} (J/mol) and the excess heat capacity C_p^{φ} (J/mol/K) being well-behaved functions of the temperature, a Taylor expansion in powers of $(T - \theta)$, where θ is a reference temperature (usually chosen as 25°C), could be applied as:

$$\Delta H^{\varphi}(T) = \Delta H^{\varphi}(\theta) + \left(C_p^{\varphi}\right)_{\theta}(T-\theta) + \frac{1}{2}\left(\frac{\partial C_p^{\varphi}}{\partial T}\right)_{\theta}(T-\theta)^2 + \frac{1}{6}\left(\frac{\partial^2 C_p^{\varphi}}{\partial T^2}\right)_{\theta}(T-\theta)^3 + \ldots \quad \text{(Equation 18)}$$

The Gibbs–Helmholtz equation gives the variations of the activity coefficient as a function of temperature from the enthalpy of mixing:

$$\Delta H^{\varphi} = \left[\frac{\partial(G^{\varphi}/T)}{\partial(1/T)}\right]_{P,b}, \quad \text{(Equation 19)}$$

Therefore, the temperature dependence of the activity and osmotic coefficients is not an expansion in $(1/k!)(T-\theta)^k$, as for the enthalpy, but rather in $(1/k!)\int_{\theta}^{T}(T-\theta)^k dT/\theta^2$.

Furthermore, the relationship demonstrated in Clarke and Glew (1966), explicited in a more complete form in Clarke and Glew (1985) showed that one could introduce the variable $x = (T-\theta)/\theta$ to express the integration as:

$$\frac{1}{k!}\int_{\theta}^{T}\frac{(T-\theta)^k}{T^2}dT = \frac{\theta^{k-2}}{(k-1)!}x^k\sum_{n=1}^{\infty}\frac{n}{n-k+1}(-x)^{n-1}\,\forall k \in \mathbb{N}^* \quad \text{(Equation 20)}$$

an expression which is explicited in the temperature matrices given in Appendix.

Matrix expression

Expressions for the activity coefficient, the molal enthalpy of mixing and the excess heat capacity of solution as a function of both composition and temperature are better represented in matrix form as

$$\gamma_s = B_{\gamma}VT_{\gamma} \quad \text{(Equation 21)}$$
$$\varphi = B_{\varphi}VT_{\varphi} \quad \text{(Equation 22)}$$
$$C_p^{\varphi} = B_C VT_C \quad \text{(Equation 23)}$$
$$\Delta H^{\varphi} = B_H VT_H \quad \text{(Equation 24)}$$

where the B_i matrices are arrays of molality terms which represent the interactions between the species in solution, explicited through the virial expansion as introduced in Equations 15–17, and the T_i matrixes are temperature arrays, explicited through the Taylor expansion as introduced in Equations 18–20. A complete expression of these matrixes can be found in B.

V is a matrix of virial coefficients of the form

$$V = \begin{pmatrix} A_0 & A_1 & A_2 & A_3 & \ldots \\ Q_0 & Q_1 & Q_2 & Q_3 & \ldots \\ B_0 & B_1 & B_2 & B_3 & \ldots \\ C_0 & C_1 & C_2 & C_3 & \ldots \\ \ldots & \ldots & \ldots & \ldots & \ldots \end{pmatrix}, \quad \text{(Equation 25)}$$

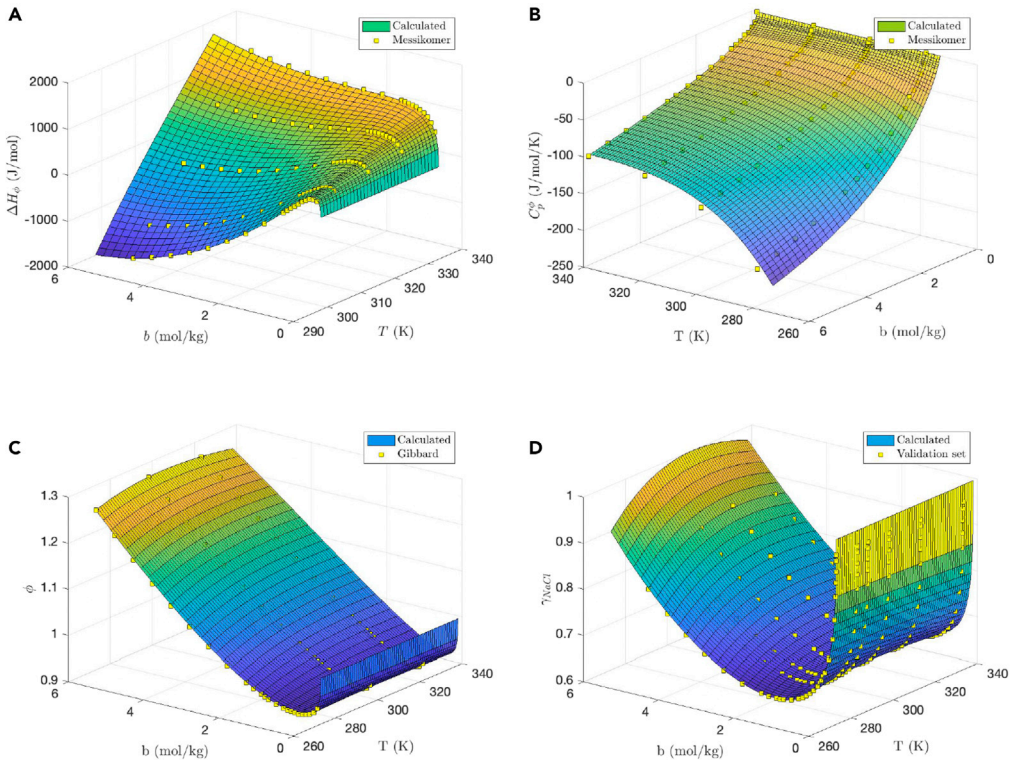

Figure 2. Graphs showing the agreement between (A) excess enthalpy (B) excess heat capacity (C) osmotic coefficient and (D) activity coefficient of NaCl(aq) as a function of molality *b* and temperature *T*, as predicted from Clarke's calculated virial matrix (surface plot) and reference data from the literature (Gibbard et al., 1974; Messikomer and Wood, 1975; Tanner and Lamb, 1978)

where the A_i coefficients are given by the Debye-Hückel theory as computed by Clarke and Glew (1980) and the $Q_i \ldots E_i$ coefficients are semi-empirical Pitzer coefficients fitted to available experimental data. This data may include colligative properties of non-ideal aqueous solutions such as vapor pressure, enthalpy of mixing, heat capacity or freezing point depression, as a function of composition

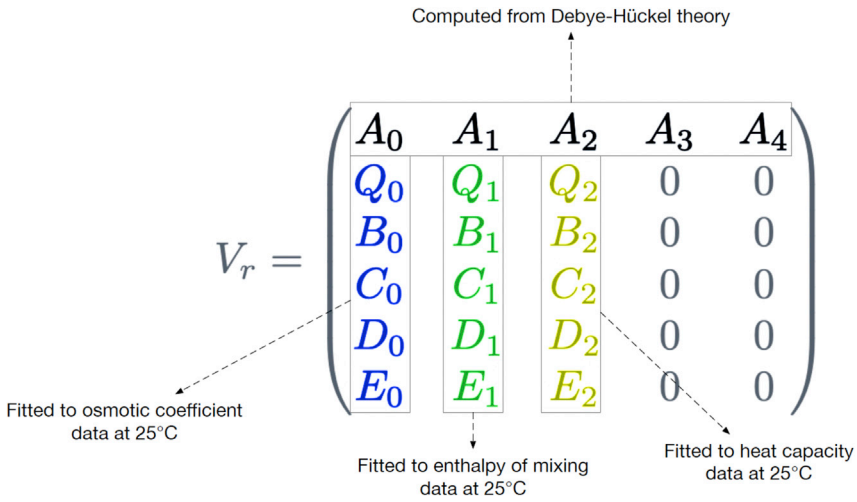

Figure 3. Graphical illustration of the fitting procedure for the reduced virial matrix

Table 1. Coefficients of the reduced virial matrix fitted to available experimental data on osmotic coefficients, excess enthalpy and heat capacity from the literature

Solvent-specific	A_0	A_1	A_2	A_3	A_4	Ref.
	−116.8569	59.2284	0.772533	0.0113	1.3439×10^{-4}	Clarke and Glew, 1980
	$kg^{\frac{1}{2}}.mol^{-\frac{1}{2}}K$	$kg^{\frac{1}{2}}.mol^{-\frac{1}{2}}K$	$kg^{\frac{1}{2}}.mol^{-\frac{1}{2}}$	$kg^{\frac{1}{2}}.mol^{-\frac{1}{2}}K^1$	$kg^{\frac{1}{2}}.mol^{-\frac{1}{2}}K^2$	
Fit φ(25°C)	Q_0	B_0	C_0	D_0	E_0	Ref.
NaCl	−82.9	−22.51	−0.7836	0.09402	4.742e-3	Clarke and Glew, 1985
KCl	−73.02	−11.97	−0.9969	0.2107	−9.914e-3	Snipes et al., 1975
$CaCl_2$	−497.4	−92.6	0.9724	−0.5565	0.05521	Ananthaswamy and Atkinson, 1985
	$kg\ mol^1K$	$kg\ mol^1K$	kg^2mol^2K	kg^3mol^3K	kg^4mol^4K	
Fit ΔH^{φ}(25°C)	Q_1	B_1	C_1	D_1	E_1	Ref.
NaCl	36.7	81.84	−20.5	2.17	−0.1262	Clarke and Glew, 1985
KCl	80.02	61.8	−7.998	−0.1125	0.04836	Snipes et al., 1975
$CaCl_2$	278.1	15.8	−6.714	−3.107	0.3062	Ananthaswamy and Atkinson, 1985
	$kg\ mol^1K$	$kg\ mol^1K$	kg^2mol^2K	kg^3mol^3K	kg^4mol^4K	
Fit C_p^{φ}(25°C)	Q_2	B_2	C_2	D_2	E_2	Ref.
NaCl	−0.4139	−1.723	0.4449	−0.05627	2.488e-3	Clarke and Glew, 1985
KCl	−2.028	−0.5265	−0.4449	0.2421	−0.03133	Tanner and Lamb, 1978
$CaCl_2$	0.1441	−0.6466	−0.3304	0.07392	−3.602e-3	Ananthaswamy and Atkinson, 1985
	$kg\ mol^1$	$kg\ mol^1$	kg^2mol^2	kg^3mol^3	kg^4mol^4	

and temperature. The fitting procedure and its associated experimental cost will be the focus of the next sections.

APPLICATION TO REFERENCE AQUEOUS ELECTROLYTES

Complete virial matrix for NaCl

Clarke and Glew (1985) compiled experimental data of various thermodynamic properties (activity coefficient, osmotic coefficient, solubility, heat of dilution, heat of solution, heat capacity) for aqueous sodium chloride solutions at different composition and temperatures from more than 100 references. Details on the treatment of experimental data from different techniques (isopiestic measurements, freezing point depression measurement, electromotive force of concentration cells, flow calorimetry) and their respective weighing are reported in Clarke and Glew (1985).

The result is the following matrix of virial coefficients

$$V = \begin{pmatrix} A_0 & A_1 & A_2 & A_3 & A_4 & 0 & 0 \\ Q_0 & Q_1 & Q_2 & Q_3 & Q_4 & Q_5 & Q_6 \\ B_0 & B_1 & B_2 & B_3 & B_4 & B_5 & 0 \\ C_0 & C_1 & C_2 & C_3 & C_4 & C_5 & 0 \\ D_0 & D_1 & D_2 & D_3 & D_4 & 0 & 0 \\ E_0 & E_1 & E_2 & 0 & 0 & 0 & 0 \end{pmatrix}, \qquad \text{(Equation 26)}$$

where the A_i coefficients are given by the Debye–Hückel theory as computed by Clarke and Glew (1980) and the $Q_i \ldots E_i$ coefficients are Pitzer coefficients which values can be found in Clarke and Glew (1985). In the present work these values, as well as the theoretical expressions from Eq.(B.1)-(B.4) (in Appendix) were entered in a MATLAB R2020b function in order to evaluate the osmotic and activity coefficients, the excess enthalpy and heat capacity as a function of composition and temperature.

The validation dataset, taken from reference literature data, was compiled from Messikomer and Wood (1975) for the excess enthalpy, from Tanner and Lamb (1978) for the excess heat capacity and from Gibbard et al. (1974) for the osmotic coefficient. The resulting surface plots are given on Figure 2, which shows that the complete Virial matrix calculated by Clarke and Glew (1985) allows to accurately estimate properties of aqueous sodium chloride as reported by other authors.

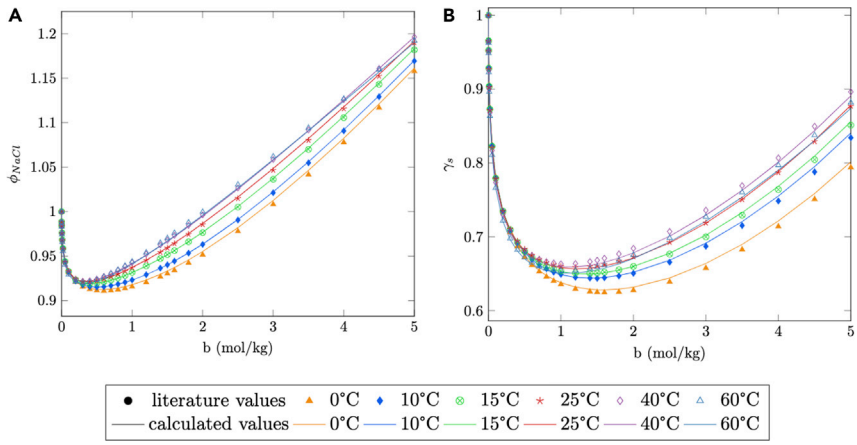

Figure 4. Reference literature values and calculated values for (A) the osmotic coefficient and (B) the activity coefficient of NaCl(aq) as a function of molality and temperature

Reduced virial matrix and fit with experimental data

The problem with the virial matrix from Clarke and Glew (1985) is the high experimental cost associated with obtaining the virial coefficients, where measurements from more than five experimental techniques are required in order to calculate accurately all Virial coefficients up to order 6. In the present section, we will demonstrate that the use of a reduced virial matrix V_r as shown in Equation (27) and Figure 3, which uses 20 virial coefficients instead of 32, results in an acceptable loss in accuracy for the estimation of osmotic and activity coefficients. As will be demonstrated in Section 4, the main interest of using the reduced virial matrix is the significant reduction in the experimental cost associated with the fitting procedure of the virial coefficients.

The reduced virial matrix is of the form

$$V_r = \begin{pmatrix} A_0 & A_1 & A_2 & A_3 & A_4 \\ Q_0 & Q_1 & Q_2 & 0 & 0 \\ B_0 & B_1 & B_2 & 0 & 0 \\ C_0 & C_1 & C_2 & 0 & 0 \\ D_0 & D_1 & D_2 & 0 & 0 \\ E_0 & E_1 & E_2 & 0 & 0 \end{pmatrix}, \qquad \text{(Equation 27)}$$

where the A_i coefficients are given by the Debye–Hückel theory as computed by Clarke and Glew (1980) and the $Q_i \ldots E_i$ coefficients are Pitzer coefficients fitted from experimental data of the excess heat capacity, enthalpy of mixing and osmotic coefficient at 25°C. As shown below, the reduced virial matrix allows a good estimation of activity coefficients, for three reference aqueous electrolytes: NaCl, KCl, and $CaCl_2$.

The fitting datasets used for calculating the virial coefficients (shown in Table 1) were taken from Clarke and Glew (1985) for NaCl, from Parker (1965), Snipes et al. (1975) for KCl, and from Ananthaswamy and Atkinson (1985) for $CaCl_2$.

The expressions at 25°C from Equations 15–17 were used to obtain the values of the reduced virial coefficients shown on Table 1. The fits gave good results, with adjusted R-square >0.9996 for all electrolytes using MATLAB R2020b curve fitting tool. Once the virial coefficients were obtained, osmotic and activity coefficients for NaCl(aq), KCl(aq) and $CaCl_2$(aq) could be calculated at different compositions and temperatures from Equation (15)-Equation (19), where the virial matrix V was replaced with the reduced virial matrix V_r introduced in Equation (27).

The obtained predicted values for the osmotic and activity coefficients for NaCl(aq), KCl(aq) and $CaCl_2$(aq) are shown on Figures 4 and 5 (lines) together with the validation datasets (dots). The residuals (in %) between predicted and references values of the osmotic and activity coefficients for NaCl(aq), KCl(aq) and $CaCl_2$(aq) are shown in C.

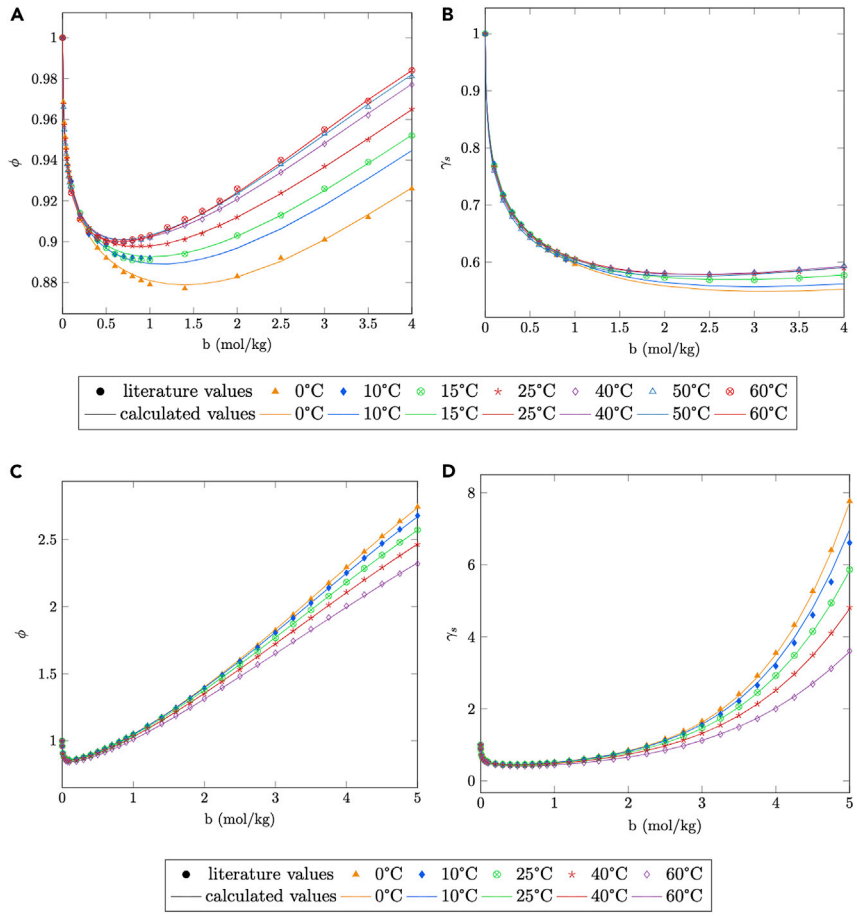

Figure 5. Agreement between reference literature values and those calculated from the reduced virial matrix for (A) the osmotic coefficient and (B) the activity coefficient for KCl(aq), and for (C) the osmotic coefficient and (D) the activity coefficient for $CaCl_2$(aq)

The validation dataset for NaCl(aq) was obtained by averaging reported values from Partanen and Partanen (2020), Gibbard et al. (1974) and Clarke and Glew (1985). Although the values reported by Partanen and Partanen (2020) were not in excellent agreement with the other reference values, a lower weight was given to this dataset.

It is apparent from Figure 4 that despite the reduction in the number of fitting coefficients, the agreement between predicted and reference values is very good on a range of molality spanning 0–5 mol/kg and a range of temperature spanning 0–60°C for NaCl(aq). The discrepancies between predicted values at different temperatures and reference literature values are given in C and show that the residuals are within [-0.43%, +0.49%] for the osmotic coefficient and [-0.92%, +1.05%] for the activity coefficient of NaCl(aq).

The validation set for KCl(aq) was taken from Snipes et al. (1975), Hostetler et al. (1967), Partanen (2016) and Hamer and Wu (1972), where, again, the dataset from Partanen et al. was given a lower weight. It is notable from Figure 5B that the calculated values are also in very good agreement with values reported in the literature, although, unfortunately, reference values for the activity coefficient of KCl(aq) at lower temperatures (0–25°C) could not be found. The discrepancies between predicted values at different temperatures and reference literature values are given in C and reveal that the residuals are within [-0.3%, +0.3%] for the osmotic coefficient and [-0.55%, +0.43%] for the activity coefficient of KCl(aq).

The validation set for $CaCl_2$(aq) was taken from Ananthaswamy and Atkinson (1985). The agreement, although less satisfactory than for the previous 1:1 electrolytes, is still good: From C we can see that the

residuals are within [−0.53%, +0.9%] for the osmotic coefficient and [−1%, +2%] for the activity coefficient. This is encouraging for the application of this method to aqueous organic 1:1 and 2:1 electrolytes such as the TEMPTMA - Methyl viologen system (Mourouga et al., 2022; Janoschka et al., 2016).

MEASUREMENT OF ACTIVITY COEFFICIENTS

In the previous section, it was demonstrated that with the knowledge of the excess enthalpy ΔH^{φ}, the excess heat capacity C_p^{φ} and the osmotic coefficient φ at a given temperature, the activity coefficient and osmotic coefficient could be calculated at any temperature with relatively good accuracy. In the present section, it will be demonstrated how differential scanning calorimetry (DSC) constitutes a rapid and efficient experimental method in the measurement of these parameters.

Differential scanning calorimetry

Differential scanning calorimetry is an experimental method where the temperature difference between an aluminum crucible containing the sample of interest (e.g., a 10 mg drop of electrolyte) and an empty, reference crucible is measured as a function of time. A linear temperature profile is imposed on the reference crucible (Figure 6A, red curve), so that when the sample holder reaches the freezing point, the exothermal freezing event results in a temperature increase in the sample holder (Figure 6A, blue curve). Similarly, on heating back to room temperature, the endothermal melting event results in a temperature decrease in the sample holder, which can be recorded and converted to units of mW/mg (Figure 6B).

It should be noted that the sample being unstirred during the experiments and the solvent being of high purity (mQ water), supercooling may occur during freezing events, so that the freezing temperature may be much lower than expected (pure water, for example, may freeze at −15°C). Supercooling is not observed on melting events, making them better suited for thermodynamic analyses.

On melting events, the location of the power peak is proportional to the melting temperature (in °C), the area under the peak to the enthalpy of melting (in J/g) and the difference between the baseline to the difference in sample heat capacity (in J/g/K) between solid and liquid state.

A method for measuring osmotic coefficients, that of freezing point depression (Lewis and Randall, 1923; Scatchard et al., 1932) allows to calculate the osmotic coefficient at the freezing point from the measurement of the freezing point of a mixture as a function of composition. Although DSC allows to measure the freezing point as well as the enthalpy and the heat capacity at the freezing point, it should be possible to derive $\varphi(T_f)$, $\Delta H^{\varphi}(T_f)$ and $C_p^{\varphi}(T_f)$ from experiments, where T_f is the freezing point of electrolyte solution. Following the reduced virial matrix method demonstrated in the previous sections, these measurements allow to calculate the activity and osmotic coefficients as a function of composition and temperature.

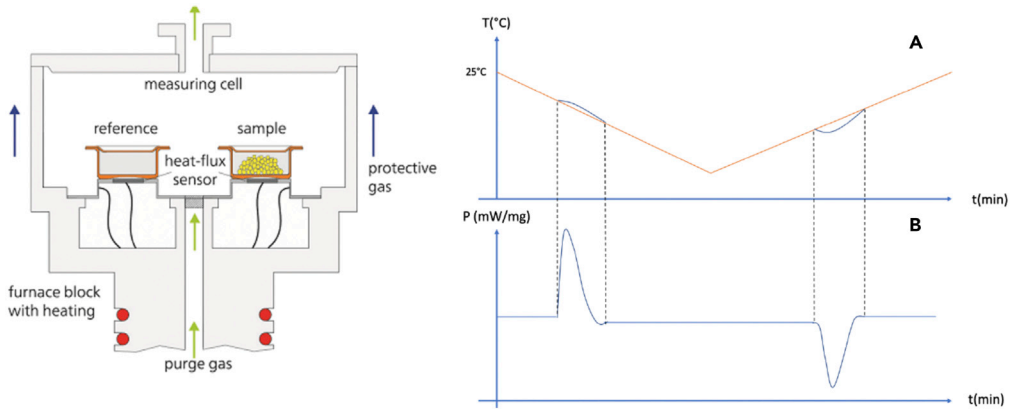

Figure 6. Illustration of a NETZSCHE differential scanning calorimeter and (A) the temperature ramp imposed on the reference crucible and the temperature recorded on the sample holder and (B) the conversion to units of mW showing exothermal freezing and endothermal melting

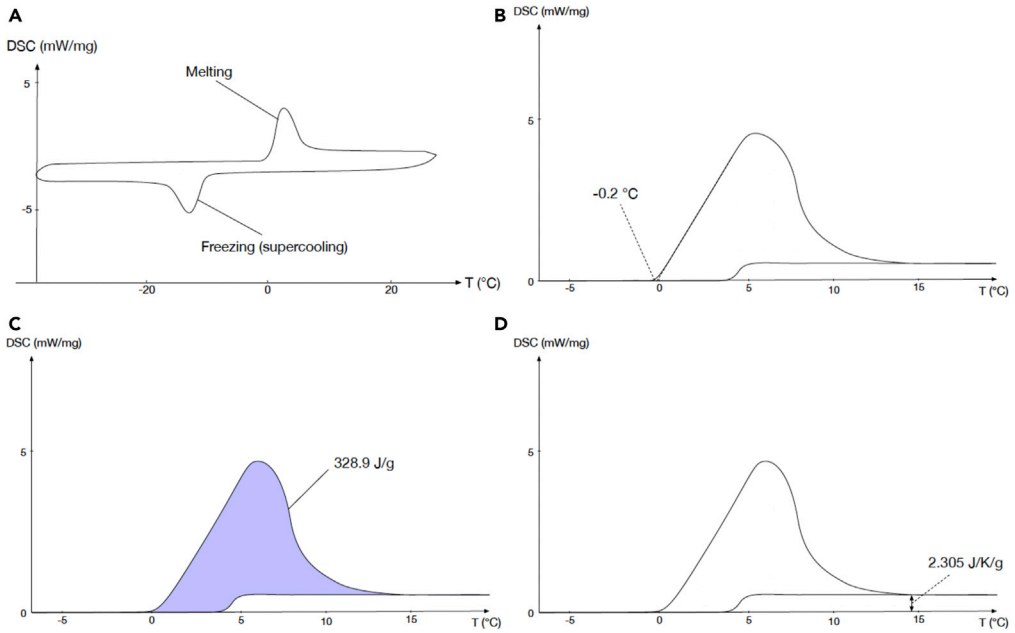

Figure 7. Graphs showing experimental DSC results on a 10 mg drop of mQ water. Endothermal events are represented with positive *y* values

Illustration on a pure substance

Differential scanning calorimetry can be performed on a 10-mg drop of pure, mQ water to illustrate the experimental outputs of the method. Figure 7 shows screenshots of DSC results from experiments performed at LRCS, Amiens, France, where it should be noted that endothermal events are represented with a positive value on the *y* axis. This is motivated by the supercooling observable on Figure 7A, where pure water freezes around −13°C, which makes freezing events unreliable, so that in the following graphs of Figure 7 only endothermal events are shown and the *y* axis is shifted accordingly to manipulate positive quantities.

Figure 7B shows the measurement of the freezing point of pure water, which is defined as the intersect between the solid-state baseline (corresponding to the heat capacity of ice) and the tangent to the first inflection point of the peak (corresponding to the maximum variation of heat capacity during the phase transition). The intersect between these slopes defines the start of the phase transition, i.e., the melting point, where DSC exhibits a 0.67% accuracy. Figure 7C shows the measurement of the area under the power curve during melting, which should correspond to the enthalpy of melting for a pure substance. For pure water, the standard enthalpy of melting is reported as 333.25 J/g, so that DSC exhibits a 1.2% accuracy. Figure 7D shows the measurement of the difference between the baselines, which should correspond to the difference between the heat capacity of the solid and the liquid phase. For pure water, the heat capacity of ice is reported as 2.1 J/g/K and the heat capacity of water as 4.2 J/g/K, so that DSC exhibits a 9.5% accuracy. It should therefore be noted that DSC is not the most accurate experimental method, and that careful uncertainty propagation should be conducted over numerical calculations parametrized with DSC results.

Illustration on a mixture

Figure 8A shows the melting peaks of DSC experiments performed on aqueous sodium chloride solutions at different compositions. Compared to a pure substance, two melting peaks are visible: the left-most one corresponds to the eutectic point of NaCl(aq) (or, equivalently, to the melting point of NaCl(sat)). The second melting point corresponds to that of the "free" water in the mixture and is therefore related to the melting point depression of NaCl(aq) as a function of composition.

Similarly to a pure substance, the area under the curve corresponds to the enthalpy of melting and the difference between the baselines to the difference in heat capacity between solid and liquid.

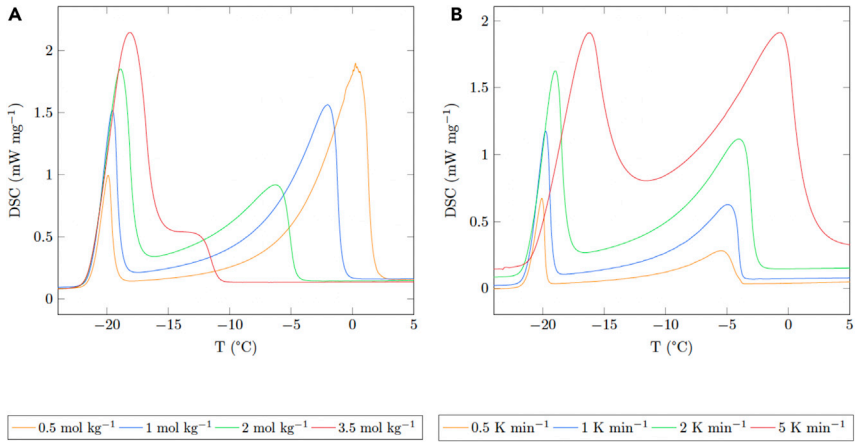

Figure 8. Melting curves for NaCl(aq) obtained via DSC (A) at different compositions for a heating rate β= 5 K/min and (B) at different heating rates for a composition of 2 mol/kg

Mixing between the saturated solution and the free water during the melting process allows to measure $\Delta H^{\varphi}(T_f)$ and $\Delta C_p^{\varphi}(T_f)$ from the DSC measurement, knowing the characteristics of the pure substances.

Limitations of the study

In the present study, it was demonstrated that activity and osmotic coefficients of aqueous mixtures of NaCl(aq), KCl(aq) and $CaCl_2$(aq) could be derived with satisfying accuracy, provided literature data on their osmotic coefficient, enthalpy of mixing and excess heat capacity were available at a reference temperature. In order to apply these methods to novel electrolytes, an experimental method using differential scanning calorimetry (DSC) was demonstrated in principle. This method, however, may suffer from the relatively high uncertainties associated with DSC.

The main difficulty arises for the measurement of the melting point T_f of aqueous mixtures, compared to that of pure substances: on the second peaks of Figure 8, the inflection point method cannot be used as the second melting peak does not exhibit an inflection point. Furthermore, Figure 8B shows the DSC curves at different heating rates. It is apparent that the heating rate has an impact on peak position and width, and therefore introduces uncertainties on the measurement of T_f, $\Delta H^{\varphi}(T_f)$ and $\Delta C_p^{\varphi}(T_f)$, due to thermal delays between the sample and the temperature sensor at the heating station.

In order to derive accurate values from the experiments, a deconvolution algorithm, allowing to reconstruct the theoretical curve at infinitely slow heating rate β= 0 should be applied. This will be the focus of our next publication focused on presenting experimental deconvoluted differential scanning calorimetry results on reference electrolyte (NaCl, KCl, and $CaCl_2$), as well as aqueous organic electrolytes for use in flow batteries (TEMPTMA chloride and methyl viologen dichloride).

Conclusion

In the present work, it was first shown that the field of flow battery modeling is increasingly questioning the validity of the dilute solution hypothesis, i.e., the fact that aqueous electrolytes behave ideally in the range of ionic strength suitable for flow battery operation. To correct this assumption, the most straightforward method is to use the concept of activity coefficient first introduced by Lewis (1907). However, very few authors provide estimated values of these activity coefficients for the aqueous electrolytes of interest in flow batteries, as a function of composition and, preferably, temperature.

We therefore demonstrated that the thermodynamic activity model developed by Pitzer (1973) and Clarke and Glew (1985) allows to calculate activity coefficients with excellent accuracy on a wide range of composition and temperature. The limitation, however, of the full Pitzer–Clarke method is the very high experimental cost associated with the calculation of all Pitzer coefficients.

A new method was therefore developed, namely the reduced virial matrix estimation, in order to reduce the experimental cost while keeping a satisfactory accuracy. The accuracy of the method was quantified with available reference literature data on activity and osmotic coefficients of common chloride electrolytes (namely NaCl(aq), KCl(aq) and $CaCl_2$(aq)).

An experimental method using differential scanning calorimetry, based on the reduced virial matrix, was presented, and its challenges outlined. In order to apply the method to aqueous flow battery electrolytes, for which activity and osmotic coefficients have not yet been reported in the literature, a deconvolution algorithm will be developed in a subsequent publication. This combined theoretical and experimental method will allow for an accurate estimation of activity coefficients for parametrizing flow battery models, at a low experimental cost.

STAR★METHODS

Detailed methods are provided in the online version of this paper and include the following:

- KEY RESOURCES TABLE
- RESOURCE AVAILABILITY
  - Lead contact
  - Materials availability
  - Data and code availability
- QUANTIFICATION AND STATISTICAL ANALYSIS
  - Gibbs free energy, chemical potential and activity coefficient
  - Kinetic theory of gases and ideal solutions
  - Activity and chemical potential in non-ideal solutions
  - Gibbs free energy of real solutions
  - MatrixForm of the virial and Taylor expansions
  - Residuals between literature references and predicted values using the reduced virial matrix

ACKNOWLEDGMENTS

This project has received funding from the European Union's Horizon 2020 research and innovation programme underGrant Agreement no. 875489 (SONAR) and 765289 (FlowCamp). We would also like to acknowledge the French Groupement de recherche RedoxFlow (GDR2070) for providing networking opportunities and facilitating cooperation.

DECLARATION OF INTERESTS

The authors declare no competing interests.

AUTHOR CONTRIBUTIONS

G.M. conducted the conceptualization of the study, its methodology, wrote the software (MATLAB code), conducted the DSC experiments, did the formal analysis as well as data curation and data visualization, and led the writing (original draft, review & editing). D.C. supported the conceptualization, methodology, formal analysis, and the writing (review & editing). E.B. supervised the conceptualization, methodology, writing (review & editing), and provided DSC experimental resources. H.R. contributed to the methodology, formal analysis, and writing (review & editing), and provided access to meeting resources. T.J.S. supervised the conceptualization and writing (review & editing). J.O.S. supervised the conceptualization, methodology, writing (review & editing), provided project administration, and was the main contributor to funding acquisition.

Received: March 2, 2022
Revised: June 13, 2022
Accepted: August 4, 2022
Published: September 16, 2022

REFERENCES

Abrams, D.S., and Prausnitz, J.M. (1975). Statistical thermodynamics of liquid mixtures: a new expression for the excess Gibbs energy of partly or completely miscible systems. AIChE J. *21*, 116–128. ISSN 1547-5905. https://doi.org/10.1002/aic.690210115. https://aiche.onlinelibrary.wiley.com/abs/10.1002/aic.690210115.

Al-Fetlawi, H., Shah, A.A., and Walsh, F.C. (2009). Non-isothermal modelling of the all-vanadium redox flow battery. Electrochim. Acta *55*, 78–89. ISSN 0013-4686. https://doi.org/10.1016/j.

electacta.2009.08.009. https://www.sciencedirect.com/science/article/pii/S0013468609010524.

Al-Yasiri, M.A. (2020). A parametric analysis of the output voltage of all-vanadium redox-flow battery system. IOP Conf. Ser. Mater. Sci. Eng. *871*, 012007. https://doi.org/10.1088/1757-899X/871/1/012007.

Amado G, E., and Blanco, L.H. (2004). Osmotic and activity coefficients of aqueous solutions of KCl at temperatures of 283.15, 288.15, 293.15 and 298.15 K: A new isopiestic apparatus. Fluid Phase Equil. *226*, 261–265. ISSN 0378-3812. https://doi.org/10.1016/j.fluid.2003.08.007. https://www.sciencedirect.com/science/article/pii/S0378381203003947.

AnanthaswamyJ and G.Atkinson. Thermodynamics of concentrated electrolyte mixtures. 5. A review of the thermodynamic properties of aqueous calcium chloride in the temperature range 273.15-373.15 K. page 9, 1985.

Ashraf Gandomi, Y., Zawodzinski, T.A., and Mench, M.M. (2014). Concentrated solution model of transport in all vanadium redox flow battery membrane separator. ECS Trans. *61*, 23–32. ISSN 1938-5862. https://doi.org/10.1149/06113.0023ecst. https://iopscience.iop.org/article/10.1149/06113.0023ecst/meta.

Badrinarayanan, R., Zhao, J., Tseng, K.J., and Skyllas-Kazacos, M. (2014). Extended dynamic model for ion diffusion in all-vanadium redox flow battery including the effects of temperature and bulk electrolyte transfer. J. Power Sources *270*, 576–586. ISSN 0378-7753. https://doi.org/10.1016/j.jpowsour.2014.07.128. https://www.sciencedirect.com/science/article/pii/S0378775314011823.

Bhattacharjee, A., and Saha, H. (2017). Design and experimental validation of a generalised electrical equivalent model of Vanadium Redox Flow Battery for interfacing with renewable energy sources. J. Energy Storage *13*, 220–232. ISSN 2352-152X. https://doi.org/10.1016/j.est.2017.07.016. https://www.sciencedirect.com/science/article/pii/S2352152X17302116.

Boettcher, P.A., Agar, E., Dennison, C.R., and Kumbur, E.C. (2015). Modeling of ion crossover in vanadium redox flow batteries: a computationally-efficient lumped parameter approach for extended cycling. J. Electrochem. Soc. *163*, A5244–A5252. ISSN 1945-7111. https://doi.org/10.1149/2.0311601jes. https://iopscience.iop.org/article/10.1149/2.0311601jes/meta.

Bradley, D.J., and Pitzer, K.S. (1979). Thermodynamics of electrolytes. 12. Dielectric properties of water and Debye-Hueckel parameters to 350.degree.C and 1 kbar. J. Phys. Chem. *83*, 1599–1603. ISSN 0022-3654. https://doi.org/10.1021/j100475a009.

Cacciuttolo, Q., Petit, M., and Pasquier, D. (2021). Fast computing flow battery modeling to optimize the choice of electrolytes and operating conditions – application to aqueous organic electrolytes. Electrochim. Acta *392*, 138961. ISSN 00134686. https://doi.org/10.1016/j.electacta.2021.138961. https://linkinghub.elsevier.com/retrieve/pii/S0013468621012512.

Chen, C.L., Yeoh, H.K., and Chakrabarti, M.H. (2014). An enhancement to Vynnycky's model for the all-vanadium redox flow battery. Electrochim. Acta *120*, 167–179. ISSN 0013-4686. https://doi.org/10.1016/j.electacta.2013.12.074. https://www.sciencedirect.com/science/article/pii/S0013468613025140.

Chen, H., Li, X., Gao, H., Liu, J., Yan, C., and Tang, A. (2019). Numerical modelling and in-depth analysis of multi-stack vanadium flow battery module incorporating transport delay. Appl. Energy *247*, 13–23. ISSN 0306-2619. https://doi.org/10.1016/j.apenergy.2019.04.034. https://www.sciencedirect.com/science/article/pii/S0306261919306671.

Chen, Q., Gerhardt, M.R., and Aziz, M.J. (2017). Dissection of the voltage losses of an acidic quinone redox flow battery. J. Electrochem. Soc. *164*, A1126–A1132. ISSN 0013-4651. https://doi.org/10.1149/2.0721706jes. https://iopscience.iop.org/article/10.1149/2.0721706jes.

Chen, Y., Bao, J., Xu, Z., Gao, P., Yan, L., Kim, S., and Wang, W. (2021a). A two-dimensional analytical unit cell model for redox flow battery evaluation and optimization. J. Power Sources *506*, 230192. ISSN 0378-7753. https://doi.org/10.1016/j.jpowsour.2021.230192. https://www.sciencedirect.com/science/article/pii/S0378775321007151.

Chen, Y., Xu, Z., Wang, C., Bao, J., Koeppel, B., Yan, L., Gao, P., and Wang, W. (2021b). Analytical modeling for redox flow battery design. J. Power Sources *482*, 228817. ISSN 03787753. https://doi.org/10.1016/j.jpowsour.2020.228817. https://linkinghub.elsevier.com/retrieve/pii/S0378775320311216.

Chu, D., Li, X., and Zhang, S. (2016). A non-isothermal transient model for a metal-free quinone–bromide flow battery. Electrochim. Acta *190*, 434–445. ISSN 434. https://doi.org/10.1016/j.electacta.2015.12.128. https://linkinghub.elsevier.com/retrieve/pii/S0013468615310501.

Clarke, E.C.W., and Glew, D.N. (1966). Evaluation of thermodynamic functions from equilibrium constants. Trans. Faraday Soc. *62*, 539–547. ISSN 0014-7672. https://doi.org/10.1039/TF9666200539.

Clarke, E.C.W., and Glew, D.N. (1985). Evaluation of the thermodynamic functions for aqueous sodium chloride from equilibrium and calorimetric measurements below 154°C. J. Phys. Chem. Ref. Data *14*, 489–610. ISSN 0047-2689. https://doi.org/10.1063/1.555730.

Clarke, E.C.W., and Glew, D.N. (1980). Evaluation of Debye–Hückel limiting slopes for water between 0 and 150°C. J. Chem. Soc., Faraday Trans.: Physical Chemistry in Condensed Phases *76*, 1911–1916. https://doi.org/10.1039/F19807601911.

Craft, Q.D., and Van Hook, W.A. (1975a). Isotope effects in aqueous systems. VI. partial molal free energies in NaCl-H2O-D2O by freezing-point measurements. The heat of fusion of D2O. J. Solut. Chem. *4*, 923–947. ISSN 1572-8927. https://doi.org/10.1007/BF00645889.

Craft, Q.D., and Van Hook, W.A. (1975b). Isotope effects in aqueous systems. V. Partial molal enthalpies of solution of NaCl-H2O-D2O and related systems (5 to 75°C)1. J. Solut. Chem. *4*, 901–922. ISSN 1572-8927. https://doi.org/10.1007/BF00645888.

Crothers, A.R., Darling, R.M., Kushner, D.I., Perry, M.L., and Weber, A.Z. (2020). Theory of multicomponent phenomena in cation-exchange membranes: Part III. Transport in vanadium redox-flow-battery separators. J. Electrochem. Soc. *167*, 013549. ISSN 1945-7111. https://doi.org/10.1149/1945-7111/ab6725.

Darken, L.S. (2002). Application of the Gibbs-Duhem Equation to Ternary and Multicomponent Systems (ACS Publications). https://doi.org/10.1021/ja01163a030. https://pubs.acs.org/pdf/10.1021/ja01163a030.

Darling, R., Gallagher, K., Xie, W., Su, L., and Brushett, F. (2016a). Transport Property requirements for flow battery separators. J. Electrochem. Soc. *163*, A5029–A5040. http://jes.ecsdl.org/content/163/1/A5029.short.

Darling, R.M., Weber, A.Z., Tucker, M.C., and Perry, M.L. (2016b). The influence of electric field on crossover in redox-flow batteries. J. Electrochem. Soc. *163*, A5014–A5022. ISSN 0013-4651. https://doi.org/10.1149/2.0031601jes. http://jes.ecsdl.org/lookup/10.1149/2.0031601jes.

del Olmo, D., Pavelka, M., and Kosek, J. (2021). Open-circuit voltage comes from non-equilibrium thermodynamics. J. Non-Equilibrium Thermodyn. *46*, 91–108. ISSN 1437-4358. https://doi.org/10.1515/jnet-2020-0070. https://www.degruyter.com/view/journals/jnet/ahead-of-print/article-10.1515-jnet-2020-0070/article-10.1515-jnet-2020-0070.xml.

Delgado, N.M., Monteiro, R., Abdollahzadeh, M., Ribeirinha, P., Bentien, A., and Mendes, A. (2020). 2D-dynamic phenomenological modelling of vanadium redox flow batteries – analysis of the mass transport related overpotentials. J. Power Sources *480*, 229142. ISSN 0378-7753. https://doi.org/10.1016/j.jpowsour.2020.229142. https://www.sciencedirect.com/science/article/pii/S0378775320314361.

Ebeling, W., and Scherwinski, K. (1983). On the estimation of theoretical individual activity coefficients of electrolytes: I. Hard sphere model. Z. Phys. Chem. ISSN 2196-7156. https://doi.org/10.1515/zpch-1983-26402.

Egner, K., Gaube, J., and Pfennig, A. (1997). GEQUAC, an excess Gibbs energy model for simultaneous description of associating and non-associating liquid mixtures. Berichte der Bunsengesellschaft für. physikalische Chemie *101*, 209–218. https://doi.org/10.1002/bbpc.19971010208.

Elgammal, R.A., Tang, Z., Sun, C.-N., Lawton, J., and Zawodzinski, T.A. (2017). Species uptake and mass transport in membranes for vanadium redox flow batteries. Electrochimica Acta *237*, 1–11. ISSN 00134686. https://doi.org/10.1016/j.electacta.2017.03.131. http://linkinghub.elsevier.com/retrieve/pii/S0013468617306138.

Cepeda, F.C. (1977). Temperature Effects on the Activity Coefficient of the Bicarbonate Ion. PhD Thesis (California Institute of Technology).

Fortier, J.L., Leduc, P.A., Picker, P., and Desnoyers, J.E. (1973). Enthalpies of dilution of electrolyte solutions by flow microcalorimetry.

J. Solution Chem. *2*, 467–475. ISSN 1572-8927. https://doi.org/10.1007/BF00651008.

Fredenslund, A., Jones, R.L., and Prausnitz, J.M. (1975). Group-contribution estimation of activity coefficients in nonideal liquid mixtures. AIChE J. *21*, 1086–1099. ISSN 0001-1541. https://doi.org/10.1002/aic.690210607.

Fedkiw, P.S., and Watts, R.W. (1984). A mathematical model for the iron/chromium redox battery. J. Electrochem. Soc. *131*, 701–709. ISSN 1945-7111. https://doi.org/10.1149/1.2115676. https://iopscience.iop.org/article/10.1149/1.2115676/meta.

Mourouga, G., Schaerer, R.P., Yang, X., Janoschka, T., Schmidt, T.J., and Schumacher, J.O. (2022). Physics-based 0D-U-I-SoC cell performance model for aqueous organic redox flow batteries. Electrochimica Acta *415*, 140185. ISSN 0013-4686. https://doi.org/10.1016/j.electacta.2022.140185. https://www.sciencedirect.com/science/article/pii/S0013468622003565.

Gandomi, Y.A., Aaron, D.S., Zawodzinski, T.A., and Mench, M.M. (2016). In Situ potential distribution measurement and validated model for all-vanadium redox flow battery. J. Electrochem. Soc. *163*, 1945–7111. ISSN 0013-4651. https://doi.org/10.1149/2.0211601jes. https://iopscience.iop.org/article/10.1149/2.0211601jes.

Gibbard, H.F., Scatchard, G., Rousseau, R.A., and Creek, J.L. (1974). Liquid-vapor equilibrium of aqueous sodium chloride, from 298 to 373.deg.K and from 1 to 6 mol kg-1, and related properties. J. Chem. Eng. Data *19*, 281–288. ISSN 0021-9568. https://doi.org/10.1021/je60062a023. https://pubs.acs.org/abs/10.1021/je60062a023.

Gibbs, J.W. (1879). On the Equilibrium of Heterogeneous Substances. Sonstiges. Volume: 2. https://archiv.ub.uni-heidelberg.de/volltextserver/13220/.

Guggenheim, E.A., and Turgeon, J.C. (1955). Specific interaction of ions. Trans. Faraday Soc. *51*, 747. ISSN 0014-7672. https://doi.org/10.1039/TF9555100747. https://pubs.rsc.org/en/content/articlelanding/1955/tf/tf9555100747.

Guggenheim, E.A., and Prue, J.E. (1954). Heats of dilution of aqueous electrolyte solutions. Trans. Faraday Soc. *50*, 710. ISSN 0014-7672. https://doi.org/10.1039/TF9545000710. https://pubs.rsc.org/en/content/articlelanding/1954/tf/tf9545000710.

Guggenheim, E. (1935). The specific thermodynamic properties of aqueous solutions of strong electrolytes. The London, Edinburgh, and Dublin Philosophical Magazine and Journal of Science *19*, 588–643. ISSN 1941-5982. https://doi.org/10.1080/14786443508561403.

Hamer, W.J., and Wu, Y.-C. (1972). Osmotic coefficients and mean activity coefficients of uni-univalent electrolytes in water at 25°C. J. Phy. Chem. Ref. Data *1*, 1047–1100. ISSN 0047-2689. https://doi.org/10.1063/1.3253108. http://aip.scitation.org/10.1063/1.3253108.

Hao, L., Wang, Y., and He, Y. (2019). Modeling of ion crossover in an all-vanadium redox flow battery with the interfacial effect at membrane/electrode interfaces. J. Electrochem. Soc. *166*, A1310–A1322. ISSN 1945-7111. https://doi.org/10.1149/2.1061906jes. https://iopscience.iop.org/article/10.1149/2.1061906jes/meta.

Hayer, N., and Kohns, M. (2020). Thermodynamically rigorous description of the open circuit voltage of redox flow batteries. J. Electrochem. Soc. *167*, 110516. ISSN 1945-7111. https://doi.org/10.1149/1945-7111/ab9e85.

Heintz, A., and Illenberger, C. (1998). Thermodynamics of vanadium redox flow batteries - electrochemical and calorimetric investigations. Berichte der Bunsengesellschaft für. physikalische Chemie *102*, 1401–1409. ISSN 0005-9021. https://doi.org/10.1002/bbpc.199800009.

Hingerl, F.F. (2012). Geothermal Electrolyte Solutions Thermodynamic Model and Computational Fitting Framework Development. PhD thesis (ETH Zürich). https://docplayer.org/83410893-Geothermal-electrolyte-solutions-thermodynamic-model-and-computational-fitting-framework-development.html.

Hostetler, P.B., Truesdell, A.H., and Christ, C.L. (1967). Activity coefficients of aqueous potassium chloride measured with a potassium-sensitive glass electrode. Science *155*, 1537–1539. https://doi.org/10.1126/science.155.3769.1537.

Howard Amanda, A., and Tartakovsky, A.M. (2021). Physics-informed CoKriging model of a redox flow battery. Preprint at arXiv. http://arxiv.org/abs/2106.09188. arXiv: 2106.09188.

Hudak, N.S. (2014). Practical thermodynamic quantities for aqueous vanadium- and iron-based flow batteries. J. Power Sources *269*, 962–974. ISSN 0378-7753. https://doi.org/10.1016/j.jpowsour.2013.12.089. https://www.sciencedirect.com/science/article/pii/S0378775313020685.

Intan, N.N., Klyukin, K., Zimudzi, T.J., Hickner, M.A., and Alexandrov, V. (2018). A combined theoretical-experimental study of interactions between vanadium ions and Nafion membrane in all-vanadium redox flow batteries. J. Power Sources *373*, 150–160. https://doi.org/10.1016/j.jpowsour.2017.10.050. https://linkinghub.elsevier.com/retrieve/pii/S0378775317313939.

Janoschka, T., Martin, N., Hager, M.D., and Schubert, U.S. (2016). An aqueous redox-flow battery with high capacity and power: the TEMPTMA/MV system. Angew. Chem. Int. Ed. Engl. *55*, 14427–14430. ISSN 1521-3773. https://doi.org/10.1002/anie.201606472.

Jones, H.C., and Getman, F.H. (1903). The molecular-lowering of the freezing-point of water produced by concentrated solutions of certain electrolytes. Zeitschrift für Physikalische Chemie *46*, 244–286. ISSN 2196-7156. https://doi.org/10.1515/zpch-1903-4619.

Klamt, A., and Schüürmann, G. (1993). COSMO: a new approach to dielectric screening in solvents with explicit expressions for the screening energy and its gradient. J. Chem. Soc. Perkin Trans. *2*, 799–805. ISSN 1364-5471. https://doi.org/10.1039/P29930000799. https://pubs.rsc.org/en/content/articlelanding/1993/p2/p29930000799.

Klamt, A., Krooshof, G.J.P., and Taylor, R. (2002). Alternative to conventional activity-coefficient models. AIChE J. *48*, 2332–2349. ISSN 1547-5905. https://doi.org/10.1002/aic.690481023.

Klamt, A. (1995). Conductor-like screening model for real solvents: a new approach to the quantitative calculation of solvation phenomena. J. Phys. Chem. *99*, 2224–2235. ISSN 0022-3654. https://doi.org/10.1021/j100007a062.

Kleinsteinberg, B., Klick, S., and Sauer, D.U. (2020). Empirical approach to determine open-circuit voltage of a vanadium-redox-flow battery for models, based on published data for anion-exchange and cation-exchange membranes and temperature dependency. Journal of Energy Storage *28*, 101109. ISSN 2352-152X. https://doi.org/10.1016/j.est.2019.101109. https://www.sciencedirect.com/science/article/pii/S2352152X19304712.

Knehr, K.W., and Kumbur, E.C. (2011). Open circuit voltage of vanadium redox flow batteries: discrepancy between models and experiments. Electrochemistry Communications *13*, 342–345. ISSN 1388-2481. https://doi.org/10.1016/j.elecom.2011.01.020. https://www.sciencedirect.com/science/article/pii/S1388248111000336.

Knehr, K.W., Agar, E., Dennison, C.R., Kalidindi, A.R., and Kumbur, E.C. (2012). A transient vanadium flow battery model incorporating vanadium crossover and water transport through the membrane. J. Electrochem. Soc. *159*, A1446–A1459. ISSN 1945-7111. https://doi.org/10.1149/2.017209jes. https://iopscience.iop.org/article/10.1149/2.017209jes/meta.

Lei, Y., Zhang, B., Bai, B., and Zhao, T. (2015). A transient electrochemical model incorporating the Donnan effect for all-vanadium redox flow batteries. Journal of Power Sources *299*, 202–211.

Lei, Y., Zhang, B.W., Zhang, Z.H., Bai, B.F., and Zhao, T.S. (2018). An improved model of ion selective adsorption in membrane and its application in vanadium redox flow batteries. Applied Energy *215*, 591–601. ISSN 03062619. https://doi.org/10.1016/j.apenergy.2018.02.042. https://linkinghub.elsevier.com/retrieve/pii/S0306261918301673.

Lewis, G.N., and Randall, M. (1923). Thermodynamics and the Free Energy of Chemical Substances (McGraw-Hill). https://books.google.fr/books?id=rW00AAAAIAAJ.

Lewis, G.N., and Randall, M. (1921). The activity coefficient of strong electrolytes. J. Am. Chem. Soc. *43*, 1112–1154. ISSN 0002-7863. https://doi.org/10.1021/ja01438a014.

Li, M., and Hikihara, T. (2008). A coupled dynamical model of redox flow battery based on chemical reaction, fluid flow, and electrical circuit. IEICE Transactions on Fundamentals of Electronics, Communications and Computer Sciences *91*, 1741–1747. ISSN 0916-8508. https://doi.org/10.1093/ietfec/e91-a.7.1741. http://joi.jlc.jst.go.jp/JST.JSTAGE/transfun/E91.A.1741?from=CrossRef.

Miller, D.G. (1963). Duhem and the Gibbs-Duhem Equation (ACS Publications). https://doi.org/10.1021/ed040p648.

Marshall, A. (1906). CXXXV.—the vapour pressures of binary mixtures. Part I. The possible types of vapour pressure curves. Journal of the Chemical Society, Transactions *89*, 1350–1386.

ISSN 0368-1645. https://doi.org/10.1039/CT9068901350.

Maurer, G., and Prausnitz, J.M. (1978). On the derivation and extension of the uniquac equation. Fluid Phase Equilibria *2*, 91–99. ISSN 0378-3812. https://doi.org/10.1016/0378-3812(78)85002-X. https://www.sciencedirect.com/science/article/pii/037838127885002X.

Messikomer, E.E., and Wood, R. (1975). The enthalpy of dilution of aqueous sodium chloride at 298.15 to 373.15 K, measured with a flow calorimeter. J. Chem. Thermodynamics *7*, 119–130. ISSN 0021-9614. https://doi.org/10.1016/0021-9614(75)90259-1. https://www.sciencedirect.com/science/article/pii/0021961475902591.

Malatesta, F. (2010). Activity coefficients of ions in sodium halide solutions: critical remarks. Fluid Phase Equilibria *295*, 244–248. ISSN 0378-3812. https://doi.org/10.1016/j.fluid.2010.05.021. http://www.sciencedirect.com/science/article/pii/S0378381210002761.

Milshtein, J.D., Tenny, K.M., Barton, J.L., Drake, J., Darling, R.M., and Brushett, F.R. (2017). Quantifying mass transfer rates in redox flow batteries. J. Electrochem. Soc. *164*, E3265–E3275. ISSN 0013-4651. https://doi.org/10.1149/2.0201711jes. http://jes.ecsdl.org/content/164/11/E3265.

Mohammadi, T., Chieng, S.C., and Skyllas Kazacos, M. (1997). Water transport study across commercial ion exchange membranes in the vanadium redox flow battery. J. Membrane Sci. *133*, 151–159. ISSN 0376-7388. https://doi.org/10.1016/S0376-7388(97)00092-6. https://www.sciencedirect.com/science/article/pii/S0376738897000926.

Moshtarikhah, S., Oppers, N.A.W., de Groot, M.T., Keurentjes, J.T.F., Schouten, J.C., and van der Schaaf, J. (2017). Nernst–Planck modeling of multicomponent ion transport in a Nafion membrane at high current density. J. Appl. Electrochem. *47*, 51–62. ISSN 1572-8838. https://doi.org/10.1007/s10800-016-1017-2.

Murali, A., Nirmalchandar, A., Krishnamoorthy, S., Hoober-Burkhardt, L., Yang, B., Soloveichik, G., Prakash, G.K.S., and Narayanan, S.R. (2018). Understanding and mitigating capacity fade in aqueous organic redox flow batteries. J. Electrochem. Soc. *165*, A1193–A1203. ISSN 0013-4651. https://doi.org/10.1149/2.0161807jes. http://jes.ecsdl.org/content/165/7/A1193.

Murthy, S.K., Sharma, A.K., Choo, C., and Birgersson, E. (2018). Analysis of concentration overpotential in an all-vanadium redox flow battery. J. Electrochem. Soc. *165*, A1746–A1752. ISSN 1945-7111. https://doi.org/10.1149/2.0681809jes. https://iopscience.iop.org/article/10.1149/2.0681809jes/meta.

Lewis, G.N. (1907). Outlines of a new system of thermodynamic chemistry. Proc. Am. Acad. Arts Sci. *43*, 259–293. ISSN 0199-9818. https://doi.org/10.2307/20022322.

Nikonenko, V.V., Vasil'eva, V.I., Akberova, E.M., Uzdenova, A.M., Urtenov, M.K., Kovalenko, A.V., Pismenskaya, N.P., Mareev, S.A., and Pourcelly, G. (2016). Competition between diffusion and electroconvection at an ion-selective surface in intensive current regimes. Adv. Colloid Interface Sci. *235*, 233–246. ISSN 00018686. https://doi.org/10.1016/j.cis.2016.06.014. http://linkinghub.elsevier.com/retrieve/pii/S000186861630118X.

Oh, K., Moazzam, M., Gwak, G., and Ju, H. (2019). Water crossover phenomena in all-vanadium redox flow batteries. Electrochimica Acta *297*, 101–111. https://doi.org/10.1016/j.electacta.2018.11.151. https://linkinghub.elsevier.com/retrieve/pii/S0013468618326355.

Parker, V.B. (1965). Thermal properties of aqueous uni-univalent electrolytes *76*.

Partanen, J.I. (2016). Mean activity coefficients and osmotic coefficients in dilute aqueous sodium or potassium chloride solutions at temperatures from (0 to 70) °C. Journal of Chemical & Engineering Data *61*, 286–306. ISSN 0021-9568. https://doi.org/10.1021/acs.jced.5b00544.

Partanen, L.J., and Partanen, J.I. (2020). Traceable values for activity and osmotic coefficients in aqueous sodium chloride solutions at temperatures from 273.15 to 373.15 K up to the saturated solutions. J. Chem. Eng. Data *65*, 5226–5239. ISSN 0021-9568. https://doi.org/10.1021/acs.jced.0c00402.

Pavelka, M., Wandschneider, F., and Mazur, P. (2015). Thermodynamic derivation of open circuit voltage in vanadium redox flow batteries. Journal of Power Sources *293*, 400–408. ISSN 0378-7753. https://doi.org/10.1016/j.jpowsour.2015.05.049. https://www.sciencedirect.com/science/article/pii/S0378775315009301.

Phutela, R.C., and Pitzer, K.S. (1986). Thermodynamics of electrolyte mixtures. Enthalpy and the effect of temperature on the activity coefficient. J. Solution Chem. *15*, 649–662. ISSN 1572-8927. https://doi.org/10.1007/BF00644597.

Pitzer, K.S. (1973). Thermodynamics of electrolytes. I. Theoretical basis and general equations. J. Phys. Chem. *77*, 268–277. ISSN 0022-3654. https://doi.org/10.1021/j100621a026.

Pitzer, K.S., and Mayorga, G. (1973). Thermodynamics of electrolytes. II. Activity and osmotic coefficients for strong electrolytes with one or both ions univalent. J. Phys. Chem. *77*, 9.

Platford Robert, F. (2002). Osmotic Coefficients of Aqueous Solutions of Seven Compounds at 0.deg (American Chemical Society). URL.

Debye, P., and Hückel, E. (1923). Zur Theorie der Elektrolyte. I. Gefrierpunktserniedrigung und verwandte Erscheinungen (Debye & Hückel). http://archive.org/details/1923-debye-huckel-theory-zur-theorie-der-elektrolyte-1.

Hückel, D.P., and Braus, M.J. (2020). The Theory of Electrolytes. I. Freezing Point Depression and Related Phenomena (Braus Translation). http://archive.org/details/1923-debye-huckel-2020-braus-translation-english.

Qiu, G., Joshi, A.S., Dennison, C., Knehr, K., Kumbur, E., and Sun, Y. (2012). 3-D pore-scale resolved model for coupled species/charge/fluid transport in a vanadium redox flow battery. Electrochimica Acta *64*, 46–64. ISSN 0013-4686. https://doi.org/10.1016/j.electacta.2011.12.065. https://www.sciencedirect.com/science/article/pii/S001346861101886X.

Reid, M.A., and Gahn, R.F. (1977). Factors Affecting the Open-Circuit Voltage and Electrode Kinetics of Some Iron/titanium Redox Flow Cells (NASA Lewis Research Center). Technical Report ERDA/NASA/1002-77/10; NASA-TM-X-73669; CONF-770531-8. https://www.osti.gov/biblio/7320222.

Ronen, R., Atlas, I., and Suss, M.E. (2018). Theory of flow batteries with fast homogeneous chemical reactions. J. Electrochem. Soc. *165*, A3820–A3827. ISSN 0013-4651. https://doi.org/10.1149/2.0251816jes.

Scatchard, G. (1936). Concentrated solutions of strong electrolytes. Chem. Rev. *19*, 309–327. ISSN 0009-2665. https://doi.org/10.1021/cr60064a008.

Scatchard, G., Jones, P.T., and Prentiss, S.S. (1932). The freezing points of aqueous solutions I. A freezing point apparatus. J. Am. Chem. Soc. *54*, 2676–2690. ISSN 0002-7863. https://doi.org/10.1021/ja01346a010.

Shah, A.A., Watt-Smith, M.J., and Walsh, F.C. (2008). A dynamic performance model for redox-flow batteries involving soluble species. Electrochimica Acta *53*, 8087–8100. ISSN 0013-4686. https://doi.org/10.1016/j.electacta.2008.05.067. https://www.sciencedirect.com/science/article/pii/S0013468608007214.

Shah, A.A., Tangirala, R., Singh, R., Wills, R.G.A., and Walsh, F.C. (2011). A dynamic unit cell model for the all-vanadium flow battery. Journal of The Electrochemical Society *158*, A671. ISSN 1945-7111. https://doi.org/10.1149/1.3561426.

Sijabat, R.R., de Groot, M.T., Moshtarikhah, S., and van der Schaaf, J. (2019). Maxwell–Stefan model of multicomponent ion transport inside a monolayer Nafion membrane for intensified chlor-alkali electrolysis. J. Appl. Electrochem. *49*, 353–368. ISSN 0021-891X. https://doi.org/10.1007/s10800-018-01283-x. http://link.springer.com/10.1007/s10800-018-01283-x.

Snipes, H.P., Manly, C., and Ensor, D.D. (1975). Heats of dilution of aqueous electrolytes. Temperature Dependence, 5.

Stephenson, D., Kim, S., Chen, F., Thomsen, E., Viswanathan, V., Wang, W., and Sprenkle, V. (2012). Electrochemical model of the Fe/V redox flow battery. J. Electrochem. Soc. *159*, A1993–A2000. http://jes.ecsdl.org/content/159/12/A1993.short.

Tanner, J.E., and Lamb, F.W. (1978). Specific heats of aqueous solutions of NaCl, NaBr, and KCl: comparisons with related thermal properties. J. Solution Chem. *7*, 303–316. ISSN 1572-8927. https://doi.org/10.1007/BF00644277.

Sukkar, T., and Skyllas-Kazacos, M. (2003). Water transfer behaviour across cation exchange membranes in the vanadium redox battery. J. Membrane Sci. *222*, 235–247. ISSN 0376-7388. https://doi.org/10.1016/S0376-7388(03)00309-0. https://www.sciencedirect.com/science/article/pii/S0376738803003090.

Tang, A., Bao, J., and Skyllas-Kazacos, M. (2011). Dynamic modelling of the effects of ion diffusion and side reactions on the capacity loss for vanadium redox flow battery. J. Power Sources *196*, 10737–10747. ISSN 0378-7753. https://doi.org/10.1016/j.jpowsour.2011.09.003.

https://www.sciencedirect.com/science/article/pii/S0378775311017095.

Tang, A., Ting, S., Bao, J., and Skyllas-Kazacos, M. (2012). Thermal modelling and simulation of the all-vanadium redox flow battery. J. Power Sources, 165–176. ISSN 0378-7753. https://doi.org/10.1016/j.jpowsour.2011.11.079. https://www.sciencedirect.com/science/article/pii/S0378775311023676.

Gür, T.M. (2018). . Review of electrical energy storage technologies, materials and systems: challenges and prospects for large-scale grid storage. Energy Environmental Science *11*, 1754–5706. ISSN 1754-5692. https://doi.org/10.1039/C8EE01419A. http://xlink.rsc.org/?DOI=C8EE01419A.

Vardner, J.T., Ye, A.A., Valdes, D.A., and West, A.C. (2020). Current-driven vanadium crossover as a function of SOC and SOD in the vanadium redox flow battery. J. Electrochem. Soc. *167*, 080512. ISSN 1945-7111. https://doi.org/10.1149/1945-7111/ab88bc. https://iopscience.iop.org/article/10.1149/1945-7111/ab88bc.

Vynnycky, M. (2011). Analysis of a model for the operation of a vanadium redox battery. Energy *36*, 2242–2256. ISSN 0360-5442. https://doi.org/10.1016/j.energy.2010.03.060. https://www.sciencedirect.com/science/article/pii/S0360544210001891.

Wandschneider, F.T., Finke, D., Grosjean, S., Fischer, P., Pinkwart, K., Tübke, J., and Nirschl, H. (2014). Model of a vanadium redox flow battery with an anion exchange membrane and a Larminie-correction. J. Power Sources *272*, 436–447. ISSN 03787753. https://doi.org/10.1016/j.jpowsour.2014.08.082. http://linkinghub.elsevier.com/retrieve/pii/S0378775314013470.

Wei, Z., Zhao, J., and Xiong, B. (2014). Dynamic electro-thermal modeling of all-vanadium redox flow battery with forced cooling strategies. Applied Energy *135*, 1–10. ISSN 0306-2619. https://doi.org/10.1016/j.apenergy.2014.08.062. https://www.sciencedirect.com/science/article/pii/S0306261914008733.

Xu, A., Shyy, W., and Zhao, T. (2017). Lattice Boltzmann modeling of transport phenomena in fuel cells and flow batteries. Acta Mech. Sin. *33*, 555–574. ISSN 1614-3116. https://doi.org/10.1007/s10409-017-0667-6.

Xu, J., Ma, Q., Xing, L., Li, H., Leung, P., Yang, W., Su, H., and Xu, Q. (2020). Modeling the effect of temperature on performance of an iron-vanadium redox flow battery with deep eutectic solvent (DES) electrolyte. J. Power Sources *449*, 227491. ISSN 0378-7753. https://doi.org/10.1016/j.jpowsour.2019.227491. https://www.sciencedirect.com/science/article/pii/S0378775319314843.

Xu, Q., and Zhao, T.S. (2015). Fundamental models for flow batteries. Progress in Energy and Combustion Science *49*, 40–58. ISSN 03601285. https://doi.org/10.1016/j.pecs.2015.02.001. http://linkinghub.elsevier.com/retrieve/pii/S036012851500012X.

Yan, Y., Li, Y., Skyllas-Kazacos, M., and Bao, J. (2016). Modelling and simulation of thermal behaviour of vanadium redox flow battery. J. Power Sources *322*, 116–128. ISSN 0378-7753. https://doi.org/10.1016/j.jpowsour.2016.05.011. https://www.sciencedirect.com/science/article/pii/S037877531630547X.

Yang, W.W., He, Y.L., and Li, Y.S. (2015). Performance modeling of a vanadium redox flow battery during discharging. Electrochimica Acta *155*, 279–287. ISSN 0013-4686. https://doi.org/10.1016/j.electacta.2014.12.138. https://www.sciencedirect.com/science/article/pii/S0013468614025973.

Yin, C., Gao, Y., Guo, S., and Tang, H. (2014). A coupled three dimensional model of vanadium redox flow battery for flow field designs. Energy *74*, 886–895. ISSN 03605442. https://doi.org/10.1016/j.energy.2014.07.066. http://linkinghub.elsevier.com/retrieve/pii/S0360544214008883.

You, D., Zhang, H., and Chen, J. (2009). A simple model for the vanadium redox battery. Electrochimica Acta *54*, 6827–6836. ISSN 6827. https://doi.org/10.1016/j.electacta.2009.06.086. http://linkinghub.elsevier.com/retrieve/pii/S0013468609009128.

Zhou, X.L., Zhao, T.S., An, L., Zeng, Y.K., and Wei, L. (2016). Modeling of ion transport through a porous separator in vanadium redox flow batteries. J. Power Sources *327*, 67–76. ISSN 0378-7753. https://doi.org/10.1016/j.jpowsour.2016.07.046. https://www.sciencedirect.com/science/article/pii/S0378775316309132.

Zhou, X.L., Zhao, T.S., An, L., Zeng, Y.K., and Yan, X.H. (2015). A vanadium redox flow battery model incorporating the effect of ion concentrations on ion mobility. Applied Energy *158*, 157–166. ISSN 03062619. https://doi.org/10.1016/j.apenergy.2015.08.028. http://linkinghub.elsevier.com/retrieve/pii/S030626191500954X.

Zawodzinski, T.A., Derouin, C., Radzinski, S., Sherman, R.J., Smith, V.T., Springer, T.E., and Gottesfeld, S. (1993). Water uptake by and transport through Nafion® 117 membranes. J. Electrochem. Soc. *140*, 1041–1047. http://jes.ecsdl.org/content/140/4/1041.short.

STAR★METHODS

KEY RESOURCES TABLE

REAGENT or RESOURCE	SOURCE	IDENTIFIER
Software and algorithms		
MATLAB code	Database: Zenodo	https://doi.org/10.5281/zenodo.6926800
Deposited data		
Experimental data compiled from lit.	Database: Mendeley Data	https://doi.org/10.17632/g4gmrwc9kg.1

RESOURCE AVAILABILITY

Lead contact

Further information and requests for resources, materials, data and code should be directed to and will be fulfilled by the lead contact, Gaël Mourouga (gaelmourouga@protonmail.com).

Materials availability

This study did not generate new unique reagents.

Data and code availability

- The publicly available data analyzed in this paper has been compiled from the literature and converted to.xlsx format. Files are available on Mendeley data: https://data.mendeley.com/datasets/g4gmrwc9kg. The DOI is listed in the key resources table, and individual publications DOI are listed in the Reference section.
- All original code has been deposited at Zenodo and is publicly available as of the date of publication. DOIs are listed in the key resources table. Executing the Matlab files, e.g. VirialMatrixNacl.m, requires some input data indicated in the first lines of the program. Note that these files should be in .txt format if the data was retrieved in .xslx format.
- Both data and original code can be retrieved from the GitHub page https://github.com/Anon75014/Thermodynamics. The Matlab files should compile directly, provided the whole folder is downloaded at once.
- Any additional information required to reanalyze the data reported in this paper is available from the lead contacton request.

QUANTIFICATION AND STATISTICAL ANALYSIS

Fitting of the reduced Virial matrix coefficients were conducted on MATLAB R2020b curve fitting tool (available on Zenodo) from selected experimental data from the literature (available on Mendeley Data). All fits yielded adjusted R-square values above 0.9996, up to 1 in most cases.

Gibbs free energy, chemical potential and activity coefficient

The Gibbs–Duhem equation states that at a specified temperature and pressure, the Gibbs free energy *G*of an aqueous solution is proportional to the chemical potential of its individual components (Miller, 1963; Darken, 2002)

$$G = \sum_i N_i \mu_i. \tag{A.1}$$

For a solute X_pY_q dissolved in water the Gibbs–Duhem equation reads

$$G = N_+\mu_+ + N_-\mu_- + N_w\mu_w, \tag{A.2}$$

where indexes + and - refer to cations and anions, respectively, and index w to water. The chemical potential of individual ions being a tricky quantity to define and manipulate (see Ebeling and Scherwinski (1983) and Malatesta (2010) for a lengthier discussion on the topic) we will conveniently introduce the chemical potential of solute

$$\mu_s = \frac{p\mu_+ + q\mu_-}{p+q} \tag{A.3}$$

and the number of moles of solute

$$N_s = \frac{N_+}{p} = \frac{N_-}{q} \tag{A.4}$$

so that

$$G = (p+q)N_s\mu_s + N_w\mu_w, \tag{A.5}$$

which is Equation (12) in Section 2.3.

Kinetic theory of gases and ideal solutions

According to the kinetic theory of gases developped by Maxwell and Boltzmann in the 1870s, the chemical potential μ^{id} of non-interacting gas molecules (ideal gases) is proportional to the logarithm of their partial molar pressure p

$$\mu^{id} = \mu^0 + RT\ln\left(\frac{p}{p^0}\right) \tag{A.6}$$

where μ^0 is the chemical potential of the gas in standard state, R is the ideal gas constant, T the absolute temperature and p^0 a reference partial pressure defined in the standard state. The same theory, applied to non-interacting ions in aqueous solutions (ideal aqueous solutions), would lead to a dependency of the chemical potential of solute μ_s^{id} in the logarithm of the molality b (in moles of solute per kilogram of solvent)

$$\mu_s^{id} = \mu_s^0 + RT\ln\left(\frac{b}{b^0}\right) \tag{A.7}$$

where b^0 represents a conventional reference molality of 1 mol/kg and μ_s^0 the chemical potential for an ideal solution in standard state. The differential from of the Gibbs–Duhem equation Equation (A.5), at constant temperature and pressure, yields

$$(p+q)N_s d\mu_s = -N_w d\mu_w, \tag{A.8}$$

so that by differentiating Equation (A.7) and noting that

$$\frac{N_s}{N_w} = \frac{b}{M_w}, \tag{A.9}$$

where M_w is the molar mass of water (expressed in kg/mol), one can obtain the following expression for the chemical potential of water

$$\mu_w^{id} = \mu_w^0 + RT(p+q)M_w b. \tag{A.10}$$

The Gibbs free energy available in an ideal solution can therefore be calculated by inserting Equation (A.7) and Equation (A.10) in Equation (12) and subtracting the Gibbs free energy in standard state $G^0 = (p+q)N_s\mu_s^0 + N_w\mu_w^0$

$$G^{id} - G^0 = (p+q)RT\left[N_w M_w b + N_s \ln\left(\frac{b}{b^0}\right)\right], \tag{A.11}$$

Activity and chemical potential in non-ideal solutions

In the case of a non-ideal solution, the chemical potential is not directly proportional to the logarithm of the molality b, but rather to the activity a_s, as introduced by Lewis (1907)

$$\mu_s = \mu_s^0 + (p+q)RT \ln a_s. \tag{A.12}$$

The activity, as mentioned before, corrects the molality of solute b by introducing an activity coefficient $\gamma_s$which accounts for the interactions between ions, as well as between the solute and the solvent. The activity is therefore defined from the molality as

$$a_s = \gamma_s \frac{b}{b^0}, \tag{A.13}$$

which leads to the following expression for the chemical potential of real solutions

$$\mu_s = \mu_s^0 + (p+q)RT \ln\left(\gamma_s \frac{b_s}{b_s^0}\right) \tag{A.14}$$

By introducing the ideal chemical potential μ_s^{id} previously defined in Equation (A.7), it is possible to express the chemical potential of real solutions as a sum of an ideal term (corresponding to the hypothetical case of ideal solutions) and an excess term μ_s^{ex} expressing the experimentally observed deviations in the behavior of real aqueous solutions

$$\mu_s = \mu_s^{id} + \mu_s^{ex} = \mu_s^{id} + RT \ln \gamma_s. \tag{A.15}$$

Similarly, the chemical potential of water can be expressed as the sum of an ideal term μ_w^{id} defined in Equation (A.10) and an excess term μ_w^{ex}. The excess term, in turn, is proportional to the osmotic coefficient φ as

$$\mu_w = \mu_w^{id} + \mu_w^{ex} = \mu_w^{id} + RT(p+q)M_w b(1-\varphi). \tag{A.16}$$

Gibbs free energy of real solutions

Defining the Gibbs free energy of the solution G as the sum of an ideal component G^{id}, corresponding to the potential energy which can be extracted from a hypothetical ideal solution, and an excess component G^{ex}, corresponding to the deviations observed from the hypothetical ideal case, we therefore obtain

$$G - G^0 = G^{id} + G^{ex}, \tag{A.17}$$

where

$$G^0 = (p+q)N_s\mu_s^0 + N_w\mu_w^0, \tag{A.18}$$

$$G^{id} = (p+q)RT\left[N_w M_w b + N_s \ln\left(\frac{b}{b^0}\right)\right], \tag{A.19}$$

$$G^{ex} = (p+q)RT(N_w M_w b(1-\varphi) + N_s \ln\gamma_s), \tag{A.20}$$

and where the partial molal Gibbs free energy G^{φ} is simply defined by normalizing the excess term with the number of moles of solute

$$G^{\varphi} = \frac{G^{ex}}{N_s}, \tag{A.21}$$

which yields Equation (14) introduced in Section 2.3

$$G^{\varphi} = (p+q)RT(1-\varphi+\ln\gamma_s). \tag{A.22}$$

Fundamentally, the excess partial molal Gibbs free energy G^{φ} captures all deviations from the hypothetical case of ideal solutions (as predicted by the kinetic theory of gases) observed in colligative properties of real aqueous solutions.

MatrixForm of the virial and Taylor expansions

The full matrix form of Equations 21–24 can be explicited as:

$$\varphi(b,T)-1=\begin{pmatrix}-|z_+z_-|\dfrac{I^{1/2}}{1+1.2I^{1/2}}\\ \left(\dfrac{2pq}{p+q}\right)e^{-2I^{1/2}}b\\ \dfrac{(2pq)}{(p+q)}b\\ \left(\dfrac{2(pq)^{3/2}}{p+q}\right)b^2\\ \left(\dfrac{2(pq)^{4/3}}{p+q}\right)b^3\\ \left(\dfrac{2(pq)^{5/4}}{p+q}\right)b^4\\ \cdots\end{pmatrix}^T V\begin{pmatrix}-\dfrac{1}{\theta}\\ \dfrac{x}{\theta}\displaystyle\sum_{n=1}^{\infty}(-x)^{n-1}\\ x^2\displaystyle\sum_{n=1}^{\infty}\frac{n}{n+1}(-x)^{n-1}\\ \dfrac{\theta}{2}x^3\displaystyle\sum_{n=1}^{\infty}\frac{n}{n+2}(-x)^{n-1}\\ \dfrac{\theta^2}{6}x^4\displaystyle\sum_{n=1}^{\infty}\frac{n}{n+3}(-x)^{n-1}\\ \cdots\end{pmatrix} \tag{B.1}$$

$$\ln\gamma(b,T)=\begin{pmatrix}-|z_+z_-|\left(\dfrac{I^{1/2}}{1+1.2I^{1/2}}+\dfrac{2}{1.2}\ln\left(1+1.2I^{1/2}\right)\right)\\ \dfrac{pq}{I(p+q)}\left(1-e^{-2I^{1/2}}\left(1+2I^{1/2}-2I\right)\right)b\\ \left(\dfrac{2pq}{p+q}\right)b\\ \dfrac{3}{2}\left(\dfrac{2(pq)^{3/2}}{p+q}\right)b^2\\ \dfrac{4}{3}\left(\dfrac{2(pq)^{2}}{p+q}\right)b^3\\ \dfrac{5}{4}\left(\dfrac{2(pq)^{5/2}}{p+q}\right)b^4\\ \cdots\end{pmatrix}^T V\begin{pmatrix}-\dfrac{1}{\theta}\\ \dfrac{x}{\theta}\displaystyle\sum_{n=1}^{\infty}(-x)^{n-1}\\ x^2\displaystyle\sum_{n=1}^{\infty}\frac{n}{n+1}(-x)^{n-1}\\ \dfrac{\theta}{2}x^3\displaystyle\sum_{n=1}^{\infty}\frac{n}{n+2}(-x)^{n-1}\\ \dfrac{\theta^2}{6}x^4\displaystyle\sum_{n=1}^{\infty}\frac{n}{n+3}(-x)^{n-1}\\ \cdots\end{pmatrix} \tag{B.2}$$

$$\Delta H^{\varphi}(b,T)=\begin{pmatrix}-|z_+z_-|\dfrac{4}{1.2}\ln\left(1+1.2I^{1/2}\right)\\ \left[1-e^{-2I^{1/2}}\left(1+2I^{1/2}\right)\right]\dfrac{b}{2I}\\ 2\dfrac{(2pq)}{(p+q)}b\\ \left(\dfrac{2(pq)^{3/2}}{p+q}\right)b^2\\ \dfrac{2}{3}\left(\dfrac{2(pq)^{4/3}}{p+q}\right)b^3\\ \cdots\end{pmatrix}^T V\begin{pmatrix}0\\ 1\\ (T-\theta)\\ \dfrac{1}{2}(T-\theta)^2\\ \dfrac{1}{6}(T-\theta)^3\\ \cdots\end{pmatrix} \tag{B.3}$$

$$C_p^{\varphi}(b,T) = \begin{pmatrix} -|z_+ z_-|\frac{4}{1.2}\ln\left(1+1.2I^{1/2}\right) \\ \left[1-e^{-2I^{1/2}}\left(1+2I^{1/2}\right)\right]\frac{b}{2I} \\ 2\frac{(2pq)}{(p+q)}b \\ \left(\frac{2(pq)^{3/2}}{p+q}\right)b^2 \\ \frac{2}{3}\left(\frac{2(pq)^{4/3}}{p+q}\right)b^3 \\ \dots \end{pmatrix}^T V \begin{pmatrix} 0 \\ 0 \\ 1 \\ (T-\theta) \\ \frac{1}{2}(T-\theta)^2 \\ \dots \end{pmatrix} \quad \text{(B.4)}$$

Residuals between literature references and predicted values using the reduced virial matrix

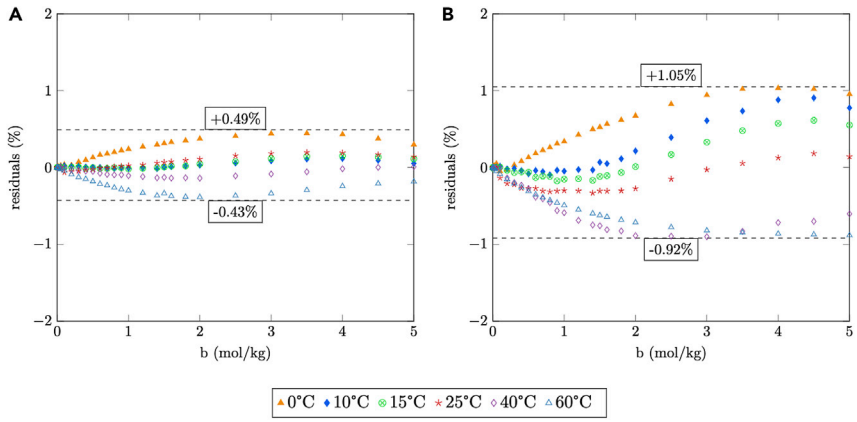

Figure 9: Residuals between reference literature values (Gibbard et al., 1974; Clarke and Glew, 1985; Partanen and Partanen, 2020) and those calculated from the reduced virial matrix for (a) the osmotic coefficient (ϕ) and (b) the activity coefficient (γ_s) of NaCl(aq) as a function of molality and temperature.

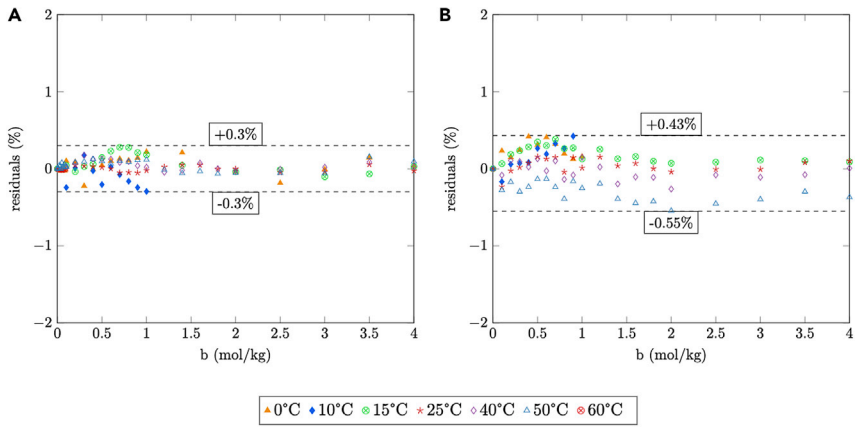

Figure 10: Residuals between reference literature values literature (Hostetler et al., 1967; Hamer and Wu, 1972; Snipes et al., 1975; Platford, 2002; Amado G and Blanco, 2004; Partanen, 2016) and those calculated from the reduced virial matrix for (a) the osmotic coefficient (ϕ) and (b) the activity coefficient (γ_s) for KCl(aq).

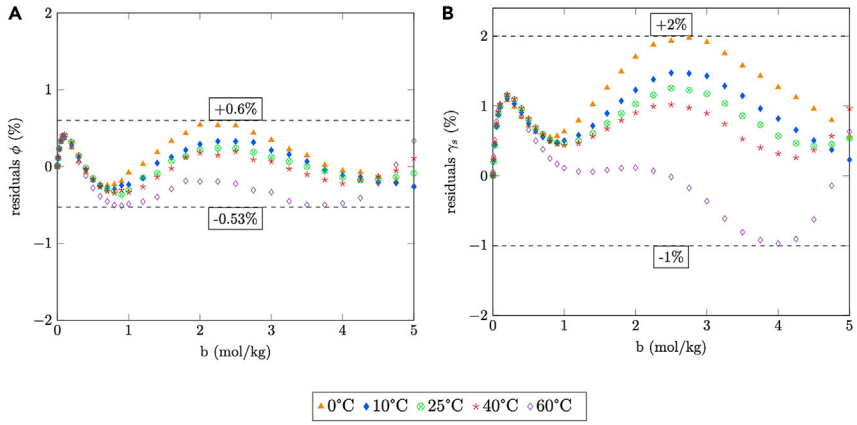

Figure 11: Residuals between reference literature values (Ananthaswamy and Atkinson, 1985) and those calculated from the reduced virial matrix for (a) the osmotic coefficient (ϕ) and (b) the activity coefficient (γ_s) for CaCl2(aq).